Study on the Substrate Recognition and the Novel Substrate Identification Method of Mn^{2+}/Mg^{2+}-dependent Ser/Thr Phosphatase PPM Family

(Mn^{2+}/Mg^{2+}依存的 Ser/Thr ホスファターゼ PPM ファミリーの基質認識と新規基質同定法に関する研究)

Graduate School of Chemical Sciences and Engineering,
Hokkaido University

Shogo Ito

2022

Table of Contents

Abbreviations

Abbreviations:

Abu	amino butyric acid
CDK9	cyclin-dependent kinase 9
DAPI	4',6-diamino-2-phenylindole dihydrochloride
EDTA	ethylenediaminetetraacetic acid
eEF2	elongation factor 2
EGTA	ethylene glycol tetraacetic acid
ERK	extracellular signal-regulated kinase
FBS	fetal bovine serum
GSK3β	glycogen synthase kinase 3β
HEPES	4-(2-hydroxyethyl)-1-piperazineethanesulfonic acid
IKKB	IκB kinase
ILKAP	Integrin-linked kinase-associated Ser/Thr phosphatase 2C
JNK	c-Jun N-terminal kinase
KO	knockout
MAPK	mitogen-activated protein kinase
MMP9	matrix metalloproteinase-9
NF-κB	nuclear factor κB
Nle	norleucine
PAGE	polyacrylamide gel electrophoresis
PP1	protein phosphatase 1
PPM	metal-dependent protein phosphatase
PP2D1	protein phosphatase 2C like domain containing 1
RelA	transcription factor p65
pS	phosphoserine
pT	phosphothreonine
PTP	ptotein tyrosine phosphatase
PTSD	post-traumatic stress disorder
pY	phosphotyrosine
SDS	sodium dodecyl sulfate
SMAD	mothers against decapentaplegic homolog
TAB1	TAK1-binding protein 1
TGF-β	transforming growth factor-β
Tris	tris(hydroxymethyl)aminomethane
VEGF	vascular endothelial growth factor
WT	wild-type

General Introduction

1.1 Metal-dependent protein phosphatase PPM

PPM is a Ser/Thr phosphatase with Mn^{2+}/Mg^{2+}-dependent dephosphorylation activity. It is a monomeric enzyme that does not require a regulatory subunit for target-specific dephosphorylation (1,2). The catalytic domain of PPM is conserved in both prokaryotes and eukaryotes. There are 20 isoforms in humans, and each isoform has a highly conserved catalytic domain and isoform-specific N-terminal, C-terminal, and loop regions (**Figure 1-1**). These isoform-specific regions have important roles for substrate recognition and functional regulation in cells. PPM phosphatase is activated by the chelation of Mn^{2+} or Mg^{2+} to essential acidic residues in the active center (**Figure 1-2**). In TAB1, the metal-chelating residues corresponding to Asp60, Asp146, Asp239, Asp243, and Asp282 of PPM1A are not conserved, and it is reported that TAB1 is a pseudo-phosphatase (3). The crystal structures of human PPM1A, PPM1B, PPM1K, PPM1H, and TAB1 have been reported, and the 3D structure of the catalytic domain is highly conserved (4–7) (**Figure 1-3**).

PPM phosphatases are involved in various and important cellular processes including proliferation, differentiation, metabolism, and immune response (1,8,9) (**Table 1-1**). In addition, it is reported that the abnormal functions of PPM cause various diseases such as cancer. PPM1D is reported to suppress the pathways of p53 tumor suppressor protein, and the overexpression of PPM1D is reported in many cancers including breast cancer and astrocytoma (10–12). Because PPM1D is a promising target for cancer therapy, many specific inhibitors for PPM1D have been developed (1,13–15). It is also reported that PPM1D is involved in the differentiation and lipid droplet formation of adipocytes and the differentiation and the maturation of neutrophils and T-cells (16–18). Our laboratory reported that the overexpression of PPM1D increases the size and number of nucleoli (19). *PPM1F* mRNA levels in human blood are lower in cases with symptoms of comorbid PTSD and depression (20). PPM1K promotes branched-chain amino acid catabolism via the dephosphorylation of the branched-chain α-keto acid dehydrogenase complex (BCKD)

(21). Expression of the inactive truncated mutant of PPM1K is reported in patients with maple syrup urine disease (22). ILKAP suppresses the anchorage-independent growth of prostate carcinoma cells via the dephosphorylation of GSK3β (23). However, the physiological functions of some PPM isoforms remain unknown, including that of PPM1J, although it is reported that PPM1J interacts with the ubiquitin-conjugating enzyme 9 (UBC9) (24). The function of PP2D1 has also not yet been clarified.

Elucidation of the physiological function of PPM is crucial for understanding the molecular mechanism of various intracellular processes. However, only a few of the cellular substrates of most PPM isoforms have been identified (**Table 1-2**). This is a major bottleneck for understanding the roles of PPM in cells.

1.2 Substrate trapping method

The comprehensive identification of substrates is a big challenge in the study of various enzymes. One of the simplest methods is to purify the stable enzyme–substrate complexes from cell lysates. In histone deacetylase (HDAC), a substrate trapping method is reported in which an inactive mutant is complexed with substrates (25). In the Tyr phosphatase PTP family, a substrate trapping method with an inactive mutant in which Cys or Asp in the active center is substituted was developed (26,27). This substrate trapping method has strongly promoted studies on PTP phosphatases. In addition, it is possible to identify the substrates of enzymes containing a regulatory subunit for substrate recognition by pull-down with the regulatory subunit. Furthermore, a substrate identification method for the ubiquitin ligase Skp1−Cul1−F-box protein (SCF) complex was reported in which the substrates are identified as proteins specifically bound to a regulatory subunit that has been mutated to inhibit binding with the catalytic subunit (28). For Ser/Thr phosphatase PP1, a substrate trapping method with the fusion protein of inactive mutant and regulatory subunit was developed (29).

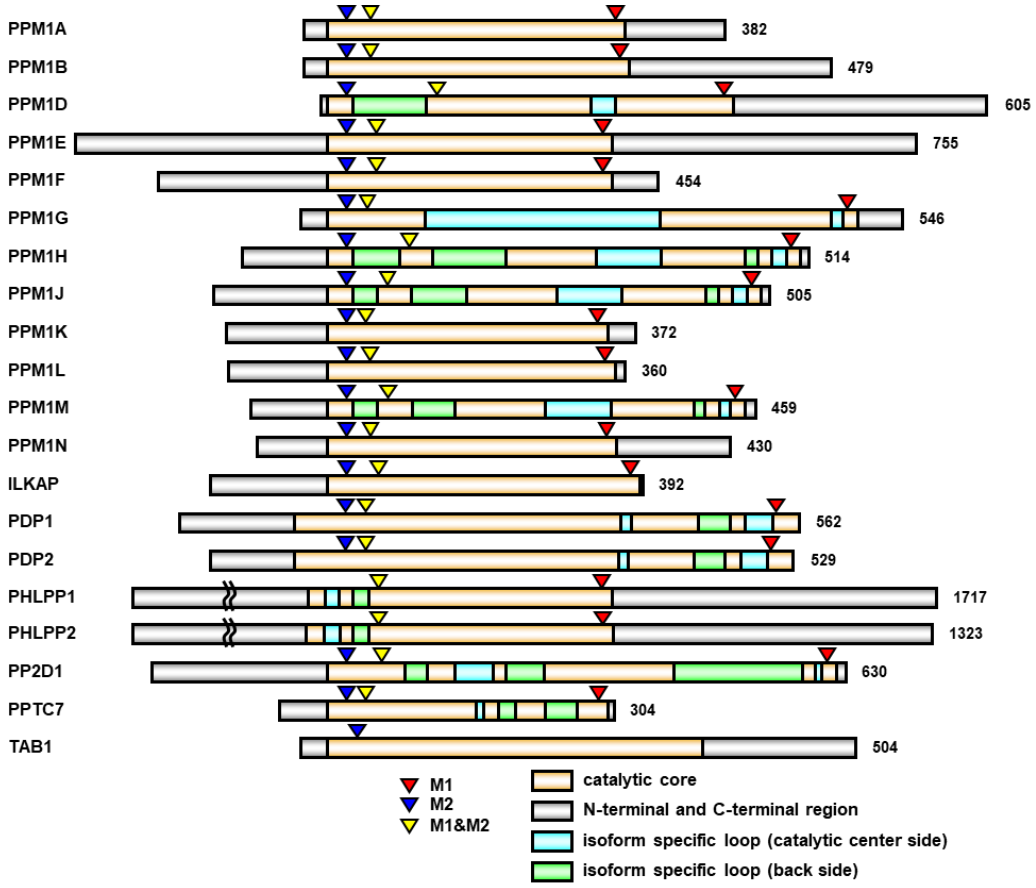

Figure 1-1. Schematic of human PPM isoform structures.

Each domain is colored as indicated. The metal-chelating residues are indicated by triangles.

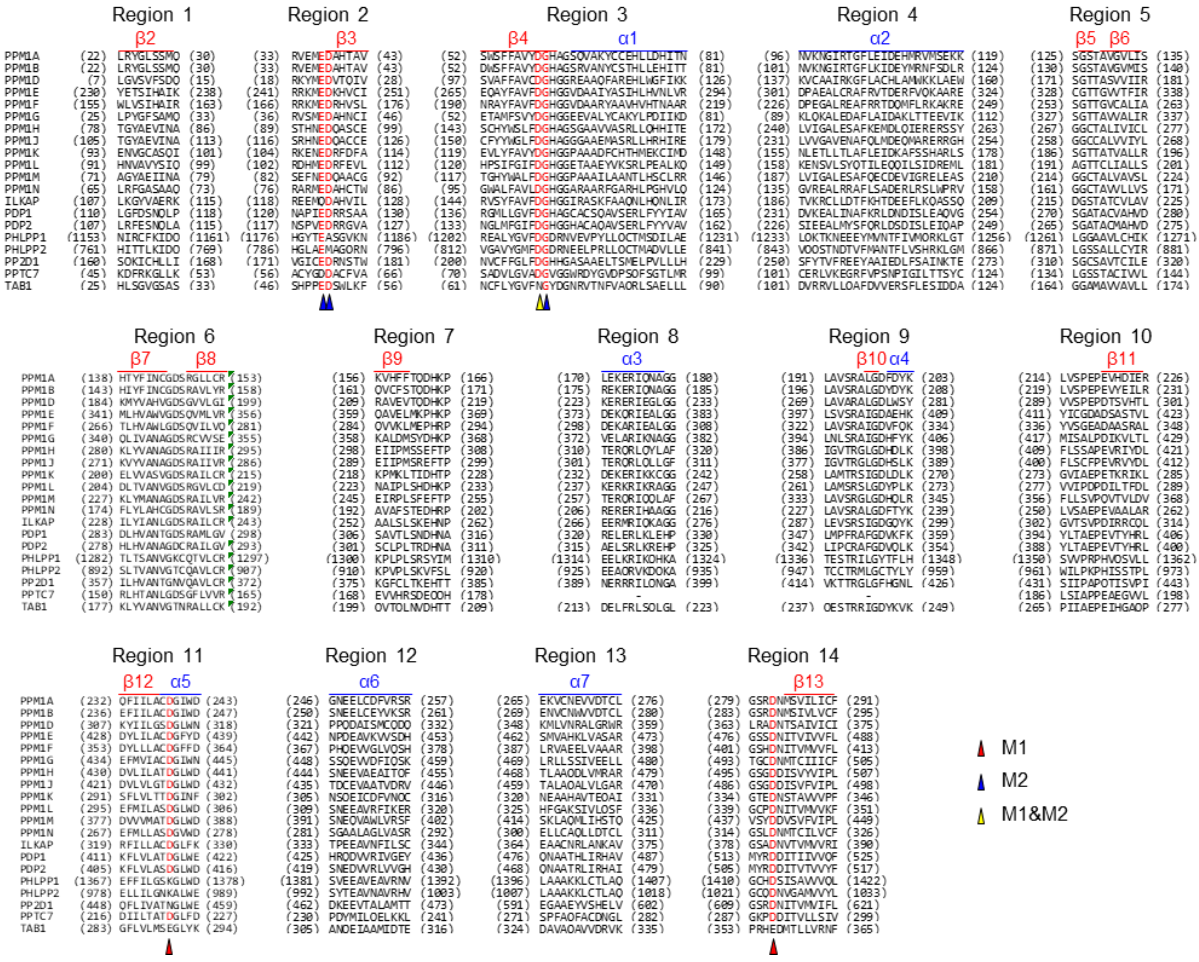

Figure 1-2. Sequence alignment of the human PPM isoforms.

Alignments were prepared by MEGA software and by visual inspection according to the crystal structure of PPM1A, PPM1B, PPM1K, PDP1 (*Rattus norvegicus*), and TAB1. The α-helices and β-strands of human PPM1A (PDB: 4RA2) are indicated in each region. The metal-chelating residues are indicated by triangles.

Table 1-1. Functions of PPM isoforms

PPM	Reports*	Physiological function	KO mouse phenotype
PPM1A	69	angiogenesis, macrophage and nerve cell differentiation, inflammation, antiviral response	re-epithelialization defet increased angiogenesis
PPM1B	27	embryonic development, necrooptosis, senescence, adipogenesis, antiviral response	embryonic lethal
PPM1D	304	immune response, metabolism, cell cycle regulation, tumorigenesis	decreased proliferation of lymphocytes testicular atrophy
PPM1E	15	tumorigenesis	-
PPM1F	32	oxidative stress response, apoptosis promotion	embryonic lethal
PPM1G	22	regulation of RNA splicing and translation, neural development	embryonic lethal
PPM1H	12	tumor suppression	loss of primary cilia
PPM1J	1	unknown	-
PPM1K	9	branched-chain amino acid metabolism	amino acid metabolism defect
PPM1L	9	adipocyte maturation, brain development	motor defect altered forebrain morphology
PPM1M	1	unknown	-
PPM1N	0	unknown	-
ILKAP	12	inhibition of anchorage-independent growth, apoptosis promotion	enhanced motor coordination
PDP1	7	pyruvate conversion to acetyl-CoA	-
PDP2	1	pyruvate conversion to acetyl-CoA	-
PHLPP1	97	light-induced resetting of the circadian clock	circadian rhythm disorder
PHLPP2	65	light-induced resetting of the circadian clock	-
PP2D1	0	unknown	-
PPTC7	2	CoQ10 biosynthesis	-
TAB1	85	(pseudo-phosphatase)	-

* Number of articles in Pubmed that include PPM and its alternative name in the title is shown (1/31/2022).

Table 1-2. Cellular substrates of PPM isoforms

PPM	Cellular substrates
PPM1A	eEF2, ERK, p38α, IKKB, YAP1, CDK9, CDK6, CDK2, Moesin, PAK1, PKCδ, mGlu3, SMAD1/2/3, AXIN1, CDC42BPA, CDC42BPB, Centrin1, PIK3R1
PPM1B	IKKB, ARHGDIA, BAD, MAP3K7, CDK9, CDK6, CDK2, Centrin1/2
PPM1D	p53, p38α, CDC25C, ATM, MDM2, CHK1/2, Histon H2AX, RSK2, RBM38, RUNX2, UNG1, PPARγ, NF-κB
PPM1E	CaMKI/IIα/IV, AMPK, PAK1
PPM1F	CaMKI/IIα/IV, AMPK, PAK1
PPM1G	DDX20, SMN1, H2AFX, HIST1H2BM, HIST1H2AG, COIL
PPM1H	CDKN1B, CSE1L
PPM1J	unknown
PPM1K	BCKDHA
PPM1L	TAK1, MEKK5, COL4A3BP
PPM1M	IKKB
PPM1N	unknown
ILKAP	HIF-1α
PDP1	PDHA1, PDHA2, SMAD1
PDP2	PDHA1, PDHA2, SMAD1
PHLPP1	AKT1/2/3, PRKCA, PRKCB, STK4, RPS6KB1
PHLPP2	AKT1/2/3, PRKCA, PRKCB, STK4, RPS6KB1
PP2D1	unknown
PPTC7	unknown
TAB1	(pseudo-phosphatase)

However, in PPM phosphatases, substitution at essential residues for activity affects the structure and electric charge of the active center because the active center is shallower than that of PTP and HDAC (**Figure 1-3**). In addition, PPM does not require a regulatory subunit for substrate recognition, and the methods for SCF complex or PP1 cannot be applied for PPM. For these reasons, there has been no report on the substrate identification method for PPM phosphatases.

The association between PPM and substrates has often been revealed through the identification of PPM as a phosphatase for protein (30,31). For example, Zhou et al. identified PPM1A as the phosphatase that downregulates the phosphorylation of Yes-associated protein (YAP) by comprehensively analyzing phosphatases, and a subsequent detailed study revealed that YAP Ser127 is the target site of PPM1A (32). The previously reported substrates of PPM were identified through this strategy but candidate substrates are limited, and it is essential to comprehensively identify the substrates of PPM for understanding the cellular functions of PPM phosphatases.

1.3 Ser/Thr phosphatase PPM1A

PPM1A is the most studied PPM isoform and is ubiquitously expressed in human tissues, whereby it is localized to the nuclei and cytoplasm in cells. It was reported that *Ppm1a* KO mice had impaired re-epithelialization process upon wounding and showed increased angiogenesis (33,34). PPM1A is well known to suppress the stimulus response through dephosphorylation of p38, ERK, and JNK related to the MAPK pathway. (35,36). Furthermore, overexpression of PPM1A in HEK293 cells causes cell cycle arrest in G2/M phase (37), suggesting that PPM1A is also involved in cell cycle regulation. PPM1A has been reported to have a tumor-suppressing role in breast and pancreatic duct adenocarcinoma (38,39). Inactivation of NF-κB by dephosphorylation of RelA at Ser276 and Ser536 has been proposed as a tumor-suppressing mechanism of PPM1A (40). PPM1A is also involved in the immune system, and it is reported that PPM1A suppresses monocyte-to-macrophage differentiation and reduces JNK phosphorylation levels to suppress apoptosis of

M. tuberculosis-infected macrophages (41,42). In T-cells, PPM1A suppresses the replication of the human immunodeficiency virus (HIV) gene via inhibition of CDK9 T-loop phosphorylation, which is the catalytic subunit of P-TEFb complex (43). PPM1A has also been reported to be involved in neuronal maturation (44). Many reports have shown that PPM1A is involved in various cellular processes, but only a few have revealed substrates of PPM1A.

PPM1A is the PPM isoform for which the most intracellular substrates have been identified. In 1993, eEF2 was identified as a substrate of PPM1A for the first time, and Thr57 and Thr59 were shown to be dephosphorylated by PPM1A (45). The phosphorylation of eEF2 at Thr57 is catalyzed by eEF2K, resulting in inhibition of the interaction between eEF2 and ribosomes and the suppression of translation (46). p38 and ERK are dephosphorylated by PPM1A at the pT-X-pY motif (Thr180 in p38 and Thr202 in ERK) (35,36,47). In HL-60 human acute myeloid leukemia cells, treatment with the PPM1A inhibitor sanguinatine increases the phosphorylation of p38 at Thr180 and promotes apoptosis (48). In addition, PPM1A suppresses the expression of TGF-β, MMP9, and VEGF via the dephosphorylation of p38 at Thr180 (34). The C-terminal SXS motif of SMAD2/3 is also a substrate of PPM1A, and the dephosphorylation of this SXS motif leads to inactivation of the TGF-β pathway (49). PPM1A can recognize various sequences as the substrate (**Table 1-3**), but the mechanism by which it does this is unclear.

1.4 Structure of PPM1A

In 1996, the crystal structure of PPM1A was reported, which was the first revealed structure of human PPM phosphatase (4). The catalytic domain of PPM1A consists of two β-sandwiches with four α-helices surrounding this β-sandwich. The catalytic center is located on the apex of the β-sandwiches and there is a structure called the FLAP domain near the active center, which is important for substrate recognition. The PPM1A-specific structure consisting of three α-helices exists at the C-terminus, but its function is unknown. At least two Mn^{2+} or Mg^{2+} coordinate in the active center. A reaction mechanism for the dephosphorylation

of PPM1A has been proposed in which water molecules trapped in these Mn^{2+}/Mg^{2+} molecules serve as nucleophiles in hydrolysis (4) (**Figure 1-4**). Tanoue et al. suggested that PPM1A chelates the third metal ion in the active center (50). The crystal structure of PPM1A shows that there are three grooves in the catalytic center, indicating that PPM1A binds to substrates in several different modes. Debnath et al. reported the crystal structure of the catalytic domain of PPM1A D146E mutant complexed with cyclic phosphopeptide (51), revealing one of the binding modes of PPM1A with its substrate. One part of PPM1A is myristoylated at the N-terminus in cells, and this modification is involved in specific substrate recognition (52).

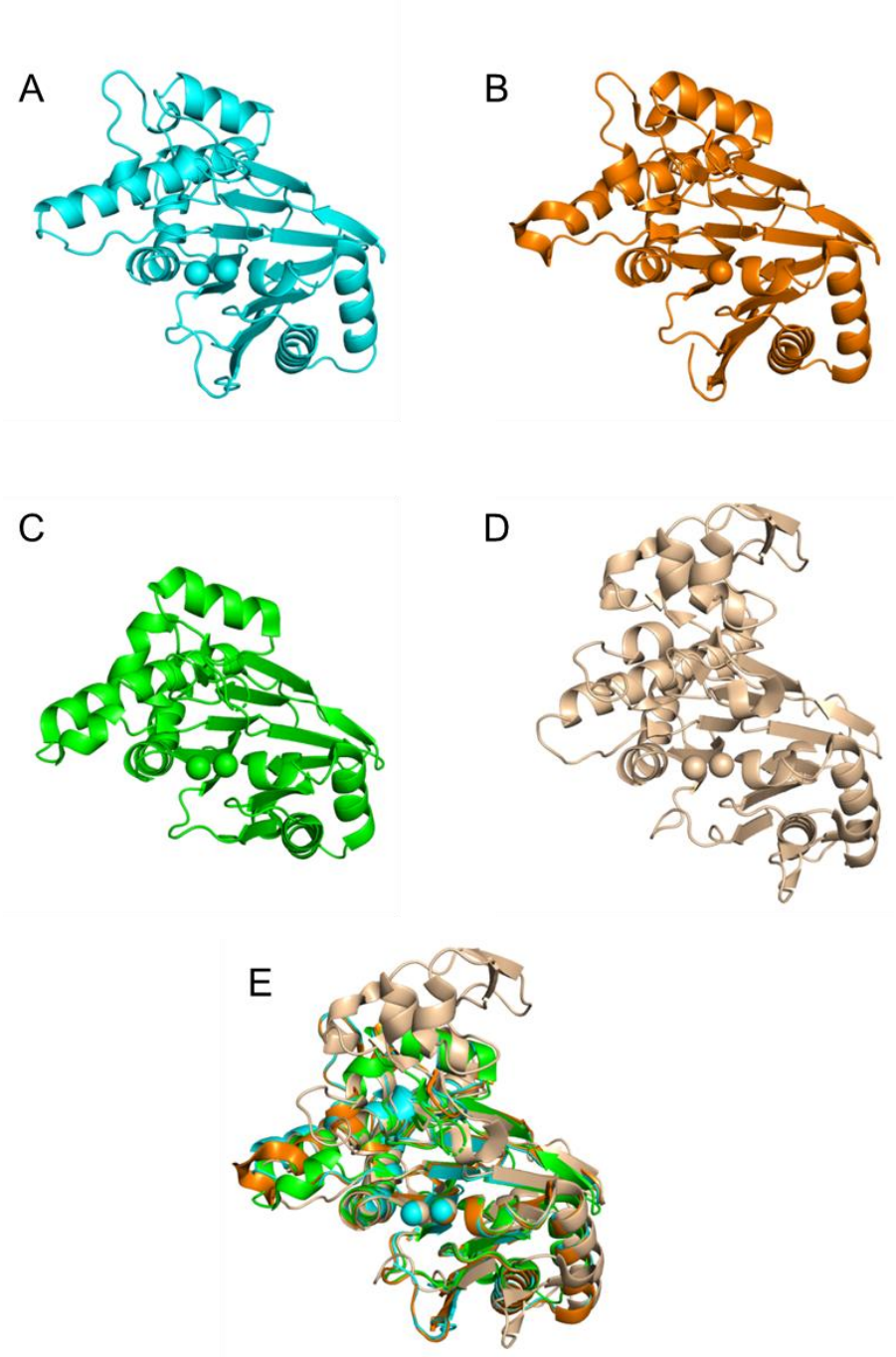

Figure 1-3. Crystal structures of the catalytic domains of PPM family members.

Ribbon model structures of PPM1A (PDB ID: 1A6Q) (A), PPM1B (PDB ID: 2P8E) (B), PPM1K (PDB ID: 4DA1) (C), and PPM1H (PDB ID: 7L4J) (D) are shown (E). These structures are superimposed.

Table 1-3. Sequences of the target sites of PPM1A

substrates	residue position											references
	-5	-4	-3	-2	-1	0	+1	+2	+3	+4	+5	
p38α(180pT)	**T**	**D**	**D**	**E**	**M**	**pT**	**G**	**pY**	**V**	**A**	**T**	(35)
ERK(175pT)	**H**	**T**	**G**	**F**	**L**	**pT**	**E**	**pY**	**V**	**A**	**T**	(36)
PAK1(198pS)	**P**	**E**	**H**	**T**	**K**	**pS**	**V**	**Y**	**T**	**R**	**S**	(53)
CDK9(186pT)	**Q**	**P**	**N**	**R**	**Y**	**pT**	**N**	**R**	**V**	**V**	**T**	(54)
CDK2(160pT)	**P**	**V**	**R**	**T**	**Y**	**pT**	**H**	**E**	**V**	**V**	**T**	(55)
CDK6(177pT)	**F**	**Q**	**M**	**A**	**L**	**pT**	**S**	**V**	**V**	**V**	**T**	(55)
mGluR3(845pS)	**H**	**L**	**N**	**R**	**F**	**pS**	**V**	**S**	**G**	**T**	**G**	(56)
PAK1(57pS)	**D**	**R**	**F**	**Y**	**R**	**pS**	**I**	**L**	**A**	**G**	**D**	(53)
eEF2(57pT)	**G**	**E**	**T**	**R**	**F**	**pT**	**D**	**T**	**R**	**K**	**D**	(45)
YAP1(127pS)	**H**	**V**	**R**	**A**	**H**	**pS**	**S**	**P**	**A**	**S**	**L**	(32)
Moesin(558pT)	**R**	**D**	**K**	**Y**	**K**	**pT**	**L**	**R**	**Q**	**I**	**R**	(57)
IKKB(181pS)	**G**	**S**	**L**	**C**	**T**	**pS**	**F**	**V**	**G**	**T**	**L**	(58)
PKCδ(507pT)	**E**	**S**	**R**	**A**	**S**	**pT**	**F**	**C**	**G**	**T**	**P**	(59)

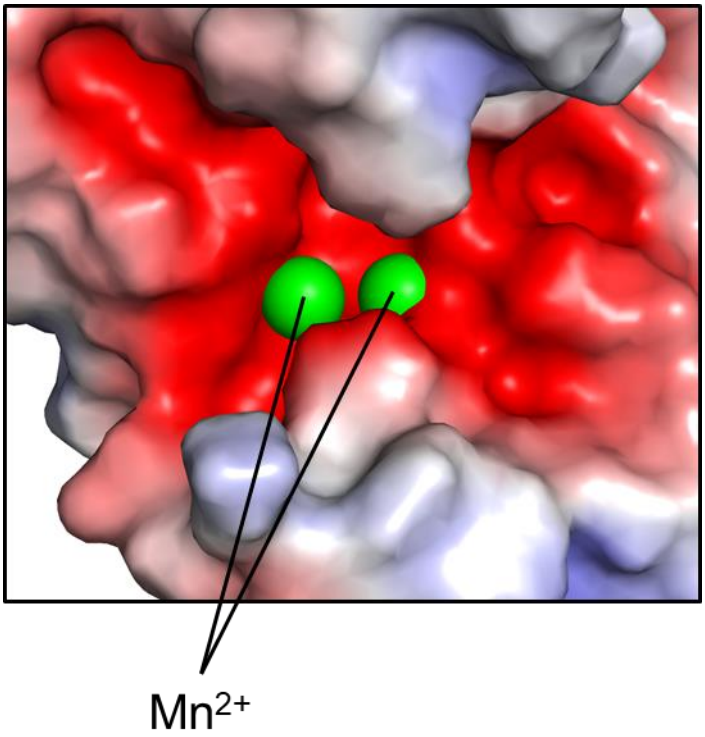

Figure 1-4. Active center of PPM1A.

The protein structure of PPM1A is shown as a surface model, and the acidic and basic regions are shown in red and blue, respectively.

1.5 Aim of this study

Only a few cellular substrates of PPM family members have been identified despite PPM having various crucial roles. The known substrates demonstrate that PPM can recognize the various sequences of the substrates. Therefore, it is essential to reveal the mechanism by which PPM recognizes substrates and to comprehensively identify these substrates to enable understanding of the physiological functions of PPM. Unlike the substrate trapping method with inactive PTP and PP1 family mutants, development of a substrate identification method with wild-type enzyme that does not affect its ability to recognize native substrates is required. In this study, PPM1A that was stable as a recombinant protein was selected as the model phosphatase. The aim of this study was to reveal the role of two arginine residues in the active center of PPM1A and to develop a novel substrate identification method that can be applied for other PPM phosphatases.

1.6 References

1. Kamada, R., *et al.* (2020) Metal-dependent Ser/Thr protein phosphatase PPM family: Evolution, structures, diseases and inhibitors. *Pharmacology & Therapeutics* **215**, 107622.
2. Shi, Y. (2009) Serine/Threonine Phosphatases: Mechanism through Structure. *Cell* **139**, 468–484.
3. Conner, S. H., *et al.* (2006) TAK1-binding protein 1 is a pseudophosphatase. *Biochemical Journal* **399**, 427–434.
4. Das, A. K., Helps, N. R., Cohen, P. T. & Barford, D. (1996) Crystal structure of the protein serine/threonine phosphatase 2C at 2.0 A resolution. *The EMBO Journal* **15**, 6798–6809.
5. Almo, S. C., *et al.* (2007) Structural genomics of protein phosphatases. *Journal of Structural and Functional Genomics* **8**, 121–140.

6. Wynn, R. M., Li, J., Brautigam, C. A., Chuang, J. L. & Chuang, D. T. (2012) Structural and Biochemical Characterization of Human Mitochondrial Branched-chain ⎵ -Ketoacid Dehydrogenase. **287**, 9178–9192.

7. Waschbüsch, D., *et al.* (2021) Structural basis for the specificity of PPM1H phosphatase for Rab GTPases. *EMBO reports* **22**, 1–22.

8. Tamura, S., *et al.* (2006) PP2C family members play key roles in regulation of cell survival and apoptosis. *Cancer Science* **97**, 563–567.

9. Gao, C., Cao, N. & Wang, Y. (2021) Metal dependent protein phosphatase PPM family in cardiac health and diseases. *Cellular Signalling* **85**, 110061.

10. Fiscella, M., *et al.* (1997) Wip1, a novel human protein phosphatase that is induced in response to ionizing radiation in a p53-dependent manner. *Proceedings of the National Academy of Sciences of the United States of America* **94**, 6048–6053.

11. Yang, H., Gao, X. Y., Li, P. & Jiang, T. S. (2015) PPM1D overexpression predicts poor prognosis in non-small cell lung cancer. *Tumor Biology* **36**, 2179–2184.

12. Zajkowicz, A., *et al.* (2015) Truncating mutations of PPM1D are found in blood DNA samples of lung cancer patients. *British Journal of Cancer* **112**, 1114–1120.

13. Ogasawara, S., *et al.* (2015) Novel inhibitors targeting PPM1D phosphatase potently suppress cancer cell proliferation. *Bioorganic and Medicinal Chemistry* **23**, 6246–6249.

14. Milosevic, J., *et al.* (2021) PPM1D Is a Therapeutic Target in Childhood Neural Tumors. 1–22.

15. Yagi, H., *et al.* (2012) A small molecule inhibitor of p53-inducible protein phosphatase PPM1D. *Bioorganic and Medicinal Chemistry Letters* **22**, 729–732.

16. Kamada, R., Kimura, N., Yoshimura, F., Tanino, K. & Sakaguchi, K. (2019) Inhibition of lipid droplet formation by Ser/Thr protein phosphatase PPM1D inhibitor, SL-176. *PLoS*

ONE **14**, 1–9.

17. Kamada, R., Kudoh, F., Yoshimura, F., Tanino, K. & Sakaguchi, K. (2017) Inhibition of Ser/Thr phosphatase PPM1D induces neutrophil differentiation in HL-60 cells. *Journal of Biochemistry* **162**, 303–308.
18. Choi, J., *et al.* (2002) Mice Deficient for the Wild-Type p53-Induced Phosphatase Gene (Wip1) Exhibit Defects in Reproductive Organs, Immune Function, and Cell Cycle Control. *Molecular and Cellular Biology* **22**, 1094–1105.
19. Kozakai, Y., *et al.* (2016) PPM1D controls nucleolar formation by up-regulating phosphorylation of nucleophosmin. *Scientific Reports* **6**, 1–11.
20. Wingo, A. P., *et al.* (2018) Expression of the PPM1F Gene Is Regulated by Stress and Associated With Anxiety and Depression. *Biological Psychiatry* **83**, 284–295.
21. Lu, G., *et al.* (2009) Protein phosphatase 2Cm is a critical regulator of branched-chain amino acid catabolism in mice and cultured cells. *J Clin Invest.* **119**, 1678–1687.
22. Oyarzabal, A., *et al.* (2013) A Novel Regulatory Defect in the Branched-Chain α-Keto Acid Dehydrogenase Complex Due to a Mutation in the PPM1K Gene Causes a Mild Variant Phenotype of Maple Syrup Urine Disease. *Human Mutation* **34**, 355–362.
23. Kumar, A. S., Naruszewicz, I., Wang, P., Leung-Hagesteijn, C. & Hannigan, G. E. (2004) ILKAP regulates ILK signaling and inhibits anchorage-independent growth. *Oncogene* **23**, 3454–3461.
24. Kashiwaba, M., *et al.* (2003) A novel protein phosphatase 2C family member (PP2Cζ) is able to associate with ubiquitin conjugating enzyme 91. *FEBS Letters* **538**, 197–202.
25. Nalawansha, D. A. & Pflum, M. K. H. (2017) LSD1 substrate binding and gene expression are affected by HDAC1-mediated deacetylation. *ACS Chemical Biology* **12**, 254–264.
26. Flint, a J., Tiganis, T., Barford, D. & Tonks, N. K. (1997) Development of "substrate-

trapping" mutants to identify physiological substrates of protein tyrosine phosphatases. *Proceedings of the National Academy of Sciences of the United States of America* **94**, 1680–1685.

27. Blanchetot, C., Chagnon, M., Dubé, N., Hallé, M. & Tremblay, M. L. (2005) Substrate-trapping techniques in the identification of cellular PTP targets. *Methods* **35**, 44–53.

28. Yumimoto, K., Matsumoto, M., Oyamada, K., Moroishi, T. & Nakayama, K. I. (2012) Comprehensive identification of substrates for f-box proteins by differential proteomics analysis. *Journal of Proteome Research* **11**, 3175–3185.

29. Wu, D., *et al.* (2018) A substrate-trapping strategy for protein phosphatase PP1 holoenzymes using hypoactive subunit fusions. **293**, 15152–15162.

30. Chen, W., *et al.* (2015) Ppm1b negatively regulates necroptosis through dephosphorylating Rip3. *Nature Cell Biology* **17**, 434–444.

31. Khoronenkova, S. V., *et al.* (2012) ATM-Dependent Downregulation of USP7/HAUSP by PPM1G Activates p53 Response to DNA Damage. *Molecular Cell* **45**, 801–813.

32. Zhou, R., *et al.* (2021) The protein phosphatase PPM1A dephosphorylates and activates YAP to govern mammalian intestinal and liver regeneration. *PLoS Biology* **19**, 1–30.

33. Yang, X., *et al.* (2011) Delayed re-epithelialization in Ppm1a gene-deficient mice is mediated by enhanced activation of Smad2. *Journal of Biological Chemistry* **286**, 42267–42273.

34. Dvashi, Z., *et al.* (2014) Protein phosphatase magnesium dependent 1A governs the wound healing-inflammation-angiogenesis cross talk on injury. *American Journal of Pathology* **184**, 2936–2950.

35. Takekawa, M., Maeda, T. & Saito, H. (1998) Protein phosphatase 2Calpha inhibits the human stress-responsive p38 and JNK MAPK pathways. *The EMBO journal* **17**, 4744–52.

36. Li, R., *et al.* (2013) Metal-dependent protein phosphatase 1A functions as an extracellular signal-regulated kinase phosphatase. *FEBS Journal* **280**, 2700–2711.

37. Ofek, P., Ben-Meir, D., Kariv-Inbal, Z., Oren, M. & Lavi, S. (2003) Cell cycle regulation and p53 activation by protein phosphatase 2Cα. *Journal of Biological Chemistry* **278**, 14299–14305.

38. Mazumdar, A., *et al.* (2019) The phosphatase PPM1A inhibits triple negative breast cancer growth by blocking cell cycle progression. *npj Breast Cancer* **5**, 1–11.

39. Fan, J., *et al.* (2016) Phosphatase PPM1A is a novel prognostic marker in pancreatic ductal adenocarcinoma. *Human Pathology* **55**, 151–158.

40. Lu, X., *et al.* (2014) PPM1A is a RelA phosphatase with tumor suppressor-like activity. *Oncogene* **33**, 2918–2927.

41. Smith, S. R., *et al.* (2018) The phosphatase PPM1A controls monocyte-to-macrophage differentiation. *Scientific Reports* **8**, 1–14.

42. Schaaf, K., *et al.* (2017) Mycobacterium tuberculosis exploits the PPM1A signaling pathway to block host macrophage apoptosis. *Scientific Reports* **7**, 1–16.

43. Budhiraja, S., Ramakrishnan, R. & Rice, A. P. (2012) Phosphatase PPM1A negatively regulates P-TEFb function in resting CD4T+ T cells and inhibits HIV-1 gene expression. *Retrovirology* **9**, 1–10.

44. Shohat, M., Ben-Meir, D. & Lavi, S. (2012) Protein phosphatase magnesium dependent 1A (PPM1A) plays a role in the differentiation and survival processes of nerve cells. *PLoS ONE* **7**, 1–11.

45. REDPATH, N. T., PRICE, N. T., SEVERINOV, K. V. & PROUD, C. G. (1993) Regulation of elongation factor‐2 by multisite phosphorylation. *European Journal of Biochemistry* **213**, 689–699.

46. Wang, X., Xie, J. & Proud, C. G. (2017) Eukaryotic elongation factor 2 kinase (eEF2K) in cancer. *Cancers* **9**, 1–15.

47. Fjeld, C. C. & Denu, J. M. (1999) Kinetic Analysis of Human SerThr Protein Phosphatase 2C α . *The Journal of Biological Chemistry* **274**, 20336–20343.

48. ABURAI, N., YOSHIDA, M., OHNISHI, M. & KIMURA, K. (2010) Sanguinarine as a Potent and Specific Inhibitor of Protein Phosphatase 2C in Vitro and Induces Apoptosis via Phosphorylation of p38 in HL60 Cells . *Bioscience, Biotechnology, and Biochemistry* **74**, 548–552.

49. Lin, X., *et al.* (2006) PPM1A Functions as a Smad Phosphatase to Terminate TGFβ Signaling. *Cell* **125**, 915–928.

50. Tanoue, K., *et al.* (2013) Binding of a third metal ion by the human phosphatases PP2Cα and Wip1 is required for phosphatase activity. *Biochemistry* **52**, 5830–5843.

51. Debnath, S., *et al.* (2018) A trapped human PPM1A–phosphopeptide complex reveals structural features critical for regulation of PPM protein phosphatase activity. *Journal of Biological Chemistry* **293**, 7993–8008.

52. Chida, T., *et al.* (2013) N-Myristoylation is essential for protein phosphatases PPM1A and PPM1B to dephosphorylate their physiological substrates in cells. *Biochemical Journal* **449**, 741–749.

53. Chan, P. M., Limsect, L. & Manser, E. (2008) PAK is regulated by PI3K, PIX, CDC42, and PP2Cα and mediates focal adhesion turnover in the hyperosmotic stress-induced p38 pathway. *Journal of Biological Chemistry* **283**, 24949–24961.

54. Wang, Y., *et al.* (2008) Phosphatase PPM1A regulates phosphorylation of Thr-186 in the Cdk9 T-loop. *Journal of Biological Chemistry* **283**, 33578–33584.

55. Cheng, A., Kaldis, P. & Solomon, M. J. (2000) Dephosphorylation of human cyclin-

dependent kinases by protein phosphatase type 2C α and β 2 isoforms. *Journal of Biological Chemistry* **275**, 34744–34749.

56. Flajolet, M., *et al.* (2003) Protein phosphatase 2C binds selectively to and dephosphorylates metabotropic glutamate receptor 3. *Proceedings of the National Academy of Sciences of the United States of America* **100**, 16006–16011.

57. Hishiya, A., Ohnishi, M., Tamura, S. & Nakamura, F. (1999) Protein phosphatase 2C inactivates F-actin binding of human platelet moesin. *Journal of Biological Chemistry* **274**, 26705–26712.

58. Sun, W., *et al.* (2009) PPM1A and PPM1B act as IKKβ phosphatases to terminate TNFα-induced IKKβ-NF-κB activation. *Cellular Signalling* **21**, 95–102.

59. Srivastava, J., Goris, J., Dilworth, S. M. & Parker, P. J. (2002) Dephosphorylation of PKCδ by protein phosphatase 2Ac and its inhibition by nucleotides. *FEBS Letters* **516**, 265–269.

2. Recognition of the substrate phosphate group in the active center of PPM1A

2.1 Abstract

The PPM family are Ser/Thr phosphatases that have various important functions in cells. Unlike many other Ser/Thr phosphatases, PPM recognizes these substrates as a monomeric enzyme. PPM1A can recognize substrates with different substrate motifs, but the detailed mechanism is unclear.

PPM1A recognizes the substrate by its active center because it does not contain an isoform-specific loop in it catalytic domain. In this study, Arg33 and Arg186 located in the vicinity of the active center were found to be involved in the dephosphorylation activity of PPM1A. Gln substitution at Arg33 reduced the PPM1A activity for the artificial substrate pNPP, whereas Gln substitution at Arg186 had little effect. However, in the dephosphorylation of the three-residue phosphopeptide Ac-Gly-pThr-Gly-NH_2, substitution at both Arg33 and Arg186 significantly reduced PPM1A activity. In addition, the effect of substitution at Arg33 and Arg186 on PPM1A activity differed depending on the sequence of the phosphopeptide. Docking model analysis revealed that Arg186 can interact with the phosphate of the substrate. These results suggested that both Arg33 and Arg186 can interact with the phosphate of the substrate and that the contribution of these arginine residues differs depending on the sequence of the substrates. Given that Arg33 and Arg186 are highly conserved in the PPM family, these findings provide new insights into the mechanism of substrate recognition by PPM.

2.2 Introduction

The PPM family consists of Mn^{2+}/Mg^{2+}-dependent Ser/Thr phosphatases and is involved in various cellular processes including proliferation, differentiation, metabolism, and immune response. The abnormal functions of PPM family proteins are reported to cause many diseases such as cancer (1,2). PPM family members are associated with many signaling pathway in cells. The PPM family does not require a regulatory subunit for substrate recognition and functions as a monomer, unlike other Ser/Thr phosphatases (1,3). PPM1A is a PPM isoform that is highly conserved from prokaryotes to eukaryotes. PPM1A is expressed in almost all tissues in humans and is located in the nuclei and cytoplasm of cells. It is reported that PPM1A has roles in angiogenesis and cell differentiation and that it functions as a tumor suppressor protein in many tumors such as breast cancer and pancreatic ductal adenocarcinoma (4–8). PPM1A dephosphorylates ERK, which regulates the mitogen-activated protein kinase (MAPK) pathway, SMAD, which responds to TGF-β signals, and IKKβ, which regulates the NF-κB pathway (9–11). PPM1A can recognize different sequences, similar to those reported for PPM1D (12). However, the mechanism by which PPM1A dephosphorylates various sequences is unclear.

The primary sequence of the catalytic domain that plays a role in the recognition and hydrolysis of the phosphate group of substrates is highly conserved in the PPM family. It was revealed by crystal structure analysis that PPM1A contains an isoform-specific region composed of three α-helixes in the C-terminus and has no loop regions in the catalytic domain, indicating that the catalytic center of PPM1A recognizes the substrate phosphate and the adjacent sequence (13). The crystal structure revealed that two divalent cations are coordinated by the acidic residues in the catalytic center. In addition to these acidic residues, two arginine residues (Arg33 and Arg186) are located in the vicinity of the divalent cations. The crystal structures of many phosphatases shows that Arg residues for the interaction with phosphate are located in the active site (14–16). In this study, the role of Arg33 and Arg186 in PPM1A was analyzed by in vitro phosphatase assay using Gln-substituted variants at Arg33 and Arg186 and docking model analysis.

2.3 Experimental procedures

2.3.1 Peptide synthesis and purification

Phosphorylated peptides from p38 (residues 176–186, 180pT, 182pY) (Ac-DDE(Nle)(pT)G(pY)VATR-NH_2), p53 (residues 15–28, 20pT) (Ac-SQETF(pT)DLWKLLPE-NH_2), and CaMKII (residues 282–292, 287pT) (Ac-WG(Nle)HRQE(pT)VE(Abu)LR-NH_2), Ac-Gly-pThr-Gly-NH_2 were synthesized using standard Fmoc solid-phase chemistry. Met179 of p38 and Cys282 of CaMKII were substituted with Nle and Abu, respectively, to avoid oxidation. Cleavage and deprotection of the side chain-protecting groups were accomplished with reagent K (TFA/water/phenol/thioanisole/ethanedithiol, 82.5:5:5:5:2.5). The crude peptides were purified by reversed-phase HPLC on a C8 column (VYDAC, Hsperia, CA) using a linear gradient of 0.05% TFA and acetonitrile, and peptide identity was confirmed by MALDI-TOF-MS (BRUKER, autoflex speed). Peptide concentrations were determined at an absorbance of 280 nm for tryptophan (molecular coefficient = 5,600) and tyrosine (molecular coefficient = 1,490) residues in the peptides.

2.3.2 Protein purification

His-tagged wild-type and Gln-substituted PPM1A were constructed using pCold I (TAKARA). His-PPM1A proteins (WT, R33Q, R186Q, R33Q/R186Q) were expressed in *E.coli* BL21(DE3) pLysS cells. The cell pellets were lysed by French press in lysis buffer (25 mM HEPES-NaOH pH7.5, 200 mM NaCl, 1 mM $MgCl_2$, and 10% glycerol). Cell debris was removed by ultracentrifugation, followed by affinity purification using TALON resin (Clontech) equilibrated in lysis buffer. His-PPM1A was eluted from the resin with an elution buffer (25 mM HEPES-NaOH pH7.5, 200 mM NaCl, 1 mM $MgCl_2$, 10% glycerol, and 150 mM imidazole), and further purified using a HiTrap Q FF (GE Healthcare) column and eluted with IEX start buffer (25 mM HEPES-NaOH pH8.0, 1 mM $MgCl_2$, 10% glycerol, and 0.005% TritonX-100) and IEX elution buffer (start buffer containing 1 M NaCl). Peak fractions were confirmed by monitoring the

dephosphorylation activity of pNPP, and a pool of fractions showing higher activity was applied to Superdex 75 (GE Healthcare) column and eluted with SEC buffer (25 mM HEPES-NaOH pH8.0, 100 mM NaCl, 1 mM $MgCl_2$, 10% glycerol, and 0.005% TritonX-100).

2.3.3 *In vitro* phosphatase assay

Assay of pNPP was performed in 50 mM Tris-HCl pH7.4, 0.1 mM EGTA, 0.02% 2-mercaptoethanol, 10 mM $MnCl_2$, and 0–20 mM pNPP with10 nM His-PPM1A mutants. All assays using phospho-peptides as substrate were performed in 50 mM Tris-HCl pH7.4, 0.1 mM EGTA, 0.02% 2-mercaptoethanol, 30 mM $MgCl_2$, 2.5–150 μM substrate peptide, and 10 nM His-PPM1A variants. K_m and k_{cat} values were calculated by fitting data points with KaleidaGraph (HULINKS) or Prism5 software (Graph Pad Software).

2.3.4 Circular Dichroism (CD) spectroscopy

Analysis was performed with 1 mM PPM1A in 10 mM HEPES-NaOH, 40 mM NaCl, 0.4 mM $MgCl_2$, and 10% glycerol at 4°C. Continuous scans were recorded by a Jasco-805 spectropolarimeter equipped with a 1-mm path length quartz cell. Spectra were obtained as the average of six different scans.

2.3.5 Computation model of PPM1A–substrate complexes

The docking modeling calculation of wild-type PPM1A complexed with the model peptide (Ac-Gly-pThr-Gly-NH_2) was performed by MOE 2011 software (Chemical Computing Group Inc.; Montreal, Canada). All salt and phosphate ions from the solvent were removed from the crystal structure of PPM1A (PDB ID: 1A6Q). The optimization of the structure with hydrogen atoms was performed with an Amber12:EHT force field. The structural model of the model peptide with the lowest energy was obtained by means of LowMode Molecular Dynamics (MD). Site Finder program was used to search for interaction

sites between PPM1A and the model peptides. The structure of the complex was obtained so that the energy was the lowest using the ASEDock program.

2.4 Results

2.4.1 Effect of R33Q and R186Q substitution on PPM1A structure and dephosphorylation activity of pNPP

Arg33 and Arg186 at the catalytic center of PPM1A were replaced with Gln, which minimized the effect of the substitution on the size and hydrophilicity of the side chain to examine the role of these arginine residues on substrate recognition. The CD spectra of three PPM1A variants, R33Q, R186Q, and R33Q/R186Q, were almost identical to that of wild-type PPM1A, indicating that these substitutions did not alter the structure (**Figure 2-1**). The effect of R33Q and R186Q substitution on the dephosphorylation activity of the artificial substrate p-nitrophenyl phosphate (pNPP) was examined. The K_m value of WT PPM1A for pNPP was 721 mM. This result was almost same as the previously reported value, 740 mM (17). R33Q and R33Q/R186Q substitution affected both the K_m and k_{cat} values and decreased the k_{cat}/K_m values by 13.5-fold compared with the WT (**Figure 2-2, Table 2-1**). The k_{cat}/K_m value of R186Q was 0.31×10^4 $s^{-1}M^{-1}$, which was virtually identical to the value of the WT. These results suggested that Arg33 has an important role in the recognition of pNPP.

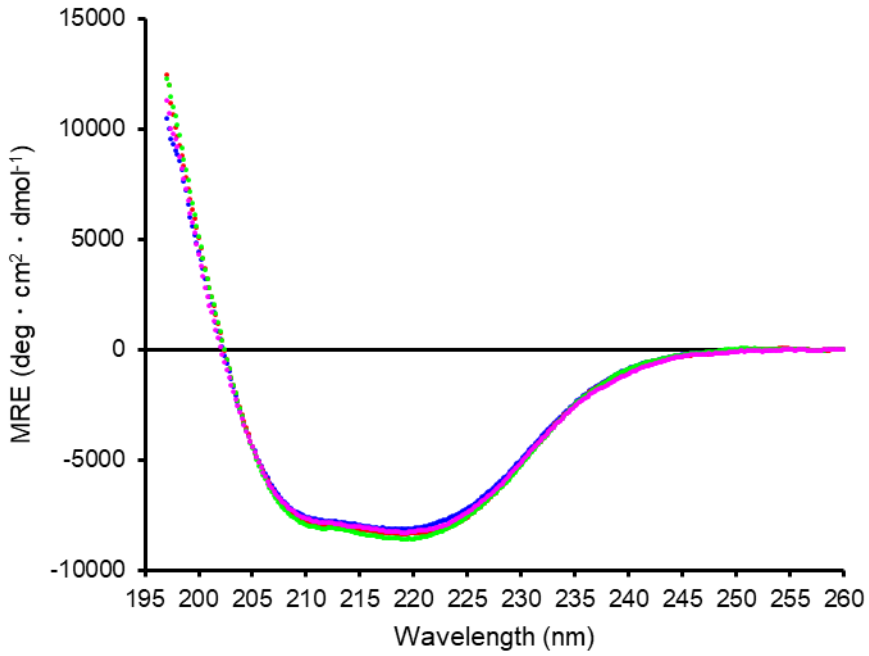

Figure 2-1. CD spectra of PPM1A variants.

The CD spectra of wild-type PPM1A, PPM1A (R33Q), PPM1A (R186Q), and PPM1A (R33Q/R186Q) are shown in blue, red, green, and magenta, respectively.

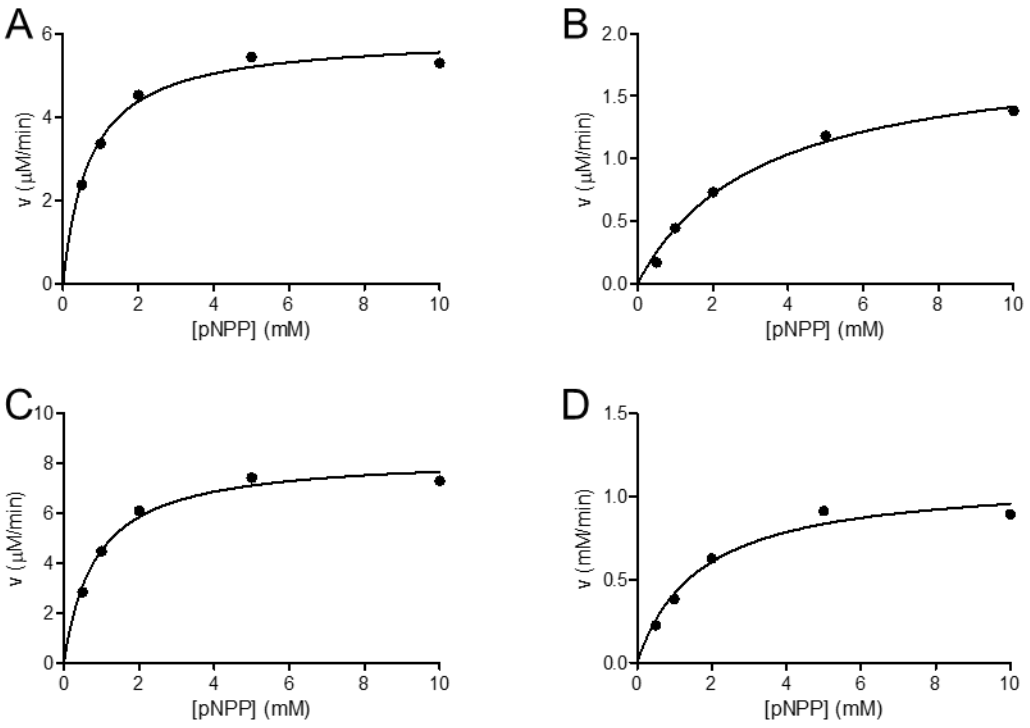

Figure 2-2. PPM1A dephosphorylation activity of p-nitrophenol (pNPP).

The velocity at each concentration of substrate was plotted. The data points were fitted to the Michaelis–Menten equation v = Vmax S/(K_m + S) by Prism5 software (Graph Pad Software). The activity of wild-type PPM1A (A), R33Q mutant (B), R186Q mutant (C), and R33Q/R186Q mutant (D) is shown.

Table 2-1. Kinetic parameters of PPM1A for pNPP

PPM1A	K_m (μM)	k_{cat} (s^{-1})	k_{cat}/K_m ($x10^4$, $s^{-1}M^{-1}$)
WT	721	1.98	0.27
R33Q	3257	0.63	0.02
R186Q	848	2.77	0.31
R33Q/R186Q	1684	0.37	0.02

2.4.2 Effect of R33Q and R186Q substitution on dephosphorylation activity of Ac-Gly-pThr-Gly-NH_2 peptide

To examine the role of Arg33 and Arg186 on the dephosphorylation of peptide substrates, the model peptide Ac-Gly-pThr-Gly-NH_2, which was designed to eliminate the effect of the side chains around the phosphorylated residue, was prepared. In the dephosphorylation of the model peptide, the K_m value of WT PPM1A was 28.0 μM, which was 28.5-fold lower than that of pNPP (**Figure 2-3, Table 2-2**). In addition, the k_{cat}/K_m value of WT PPM1A for the model peptide was 64.8-fold better than that of pNPP (**Table 2-2**). These results showed that the model peptide was much better than pNPP as a substrate for analyzing the dephosphorylation of PPM1A. Both R33Q and R186Q substitution reduced the k_{cat}/K_m values of the model peptide by 35.0-fold and 87.5-fold, respectively. The reduced k_{cat}/K_m values were due to the significant decrease in the k_{cat} values, and there was little effect on the K_m values. The dephosphorylation activity of R33Q/R186Q for the model peptide was not detected. These results suggested that both Arg33 and Arg186 have important roles in the dephosphorylation of the model peptide.

2.4.3 Effect of the sequence around the dephosphorylation site

To examine the effect of the sequence around the phosphorylated residue, PPM1A phosphatase activity for three different phosphopeptide substrates derived from p38, CaMKII, and p53 was analyzed. The K_m and k_{cat} values of CaMKII and p53 peptide were comparable to p38 peptide, which is often used as the peptide substrate of PPM1A (**Figure 2-4, Table 2-3**). The turnover of WT PPM1A was 4.40 s^{-1} for p38 peptide at 150 μM substrate, whereas the turnover of R33Q and R186Q was 0.05 s^{-1} and 0.01 s^{-1}, respectively (**Table 2-3**). The effect of the single substitution of Gln at Arg33 or Arg186 on the dephosphorylation of CaMKII and p53 peptide was moderate, although these substitutions abolished PPM1A activity in the dephosphorylation of p38 peptide. R33Q substitution had a greater effect on PPM1A activity than R186Q in

the dephosphorylation of CaMKII peptide, whereas R186Q substitution had a greater effect on the dephosphorylation of p53 peptide.

2.4.4 Docking model structure of the complex of PPM1A and Ac-Gly-pThr-Gly-NH_2 peptide

The structure of PPM1A complexed with the model peptide was obtained by docking model analysis. In the docking model structure, the distance between the Nh atom of Arg33 and the closest O atom was 4.13 Å, and the distance between the Nh atom of Arg186 and the closest O atom was 2.62 Å (**Figure 2-5A and C**). The phosphate group of the model peptide was positioned closer to Arg186 than to Arg33, consistent with the observation that R186Q showed a lower k_{cat}/K_m value than R33Q. In the reported crystal structure of the catalytic domain of PPM1A(D146E) mutant complexed with cyclic peptide containing pS-X-pY sequence, the distance between the Nh atom of Arg33 and the closest O atom was 2.61 Å, and the distance between the Nh atom of Arg186 and the closest O atom was 7.69 Å (**Figure 2-5B and D**). The distance from the Nh atom of Arg186 to the closest O atom of the model peptide in the docking model structure was almost the same as the distance from the Nh atom of Arg33 to the closest O atom of the cyclic peptide, indicating that Arg186 also interacted with the phosphate group of the substrate. In addition, it was suggested that Arg186 played a more significant role in the dephosphorylation of the model peptide than Arg33.

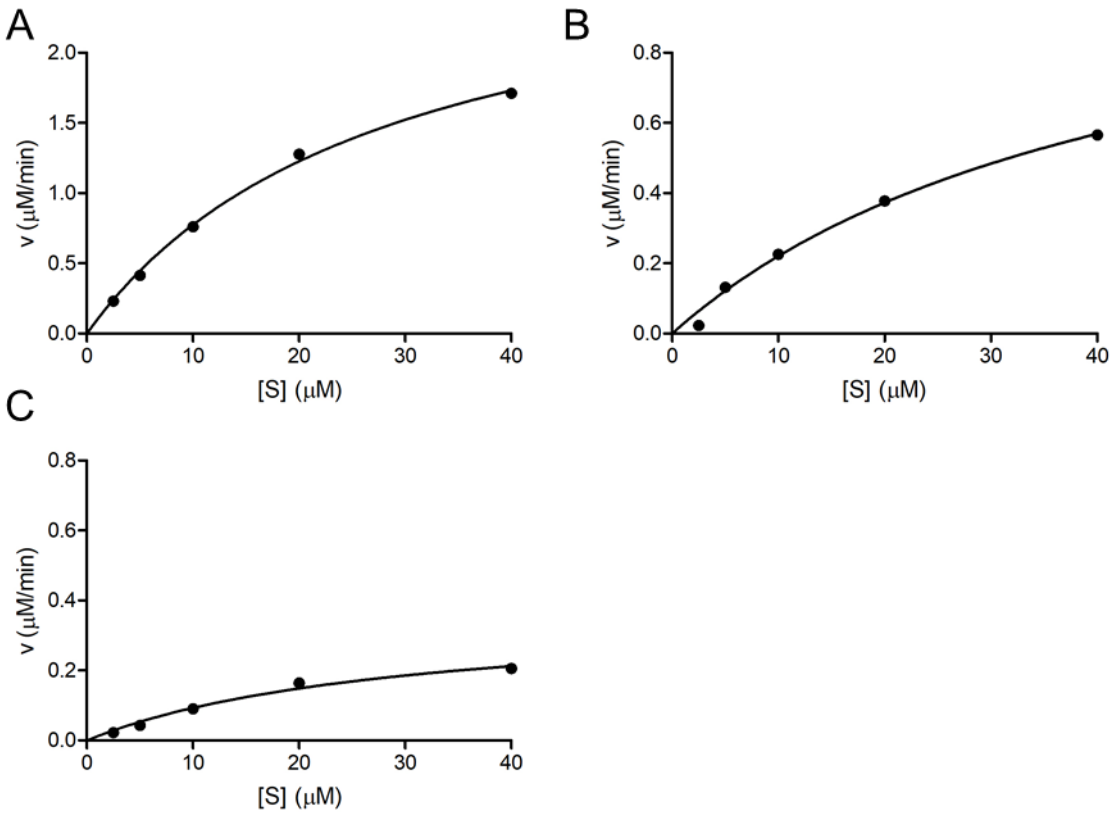

Figure 2-3. PPM1A dephosphorylation activity for Ac-Gly-pThr-Gly-NH_2.

The velocity at each concentration of substrate was plotted. The data points were fitted to the Michaelis–Menten equation v = Vmax S/(K_m + S) by Prism5 software (Graph Pad Software). The activity of wild-type PPM1A (A), R33Q mutant (B), and R186Q mutant (C) is shown.

Table 2-2. Kinetic parameters of PPM1A for the model peptide Ac-Gly-pThr-Gly-NH_2

PPM1A	K_m (μM)	k_{cat} (s^{-1})	k_{cat}/K_m ($x10^4$, $s^{-1}M^{-1}$)
WT	28.0	4.90	17.5
R33Q	44.4	0.20	0.50
R186Q	29.9	0.06	0.20
R33Q/R186Q	NA[a]	NA[a]	NA[a]

[a] NA, not active. Unable to determine kinetic parameters.

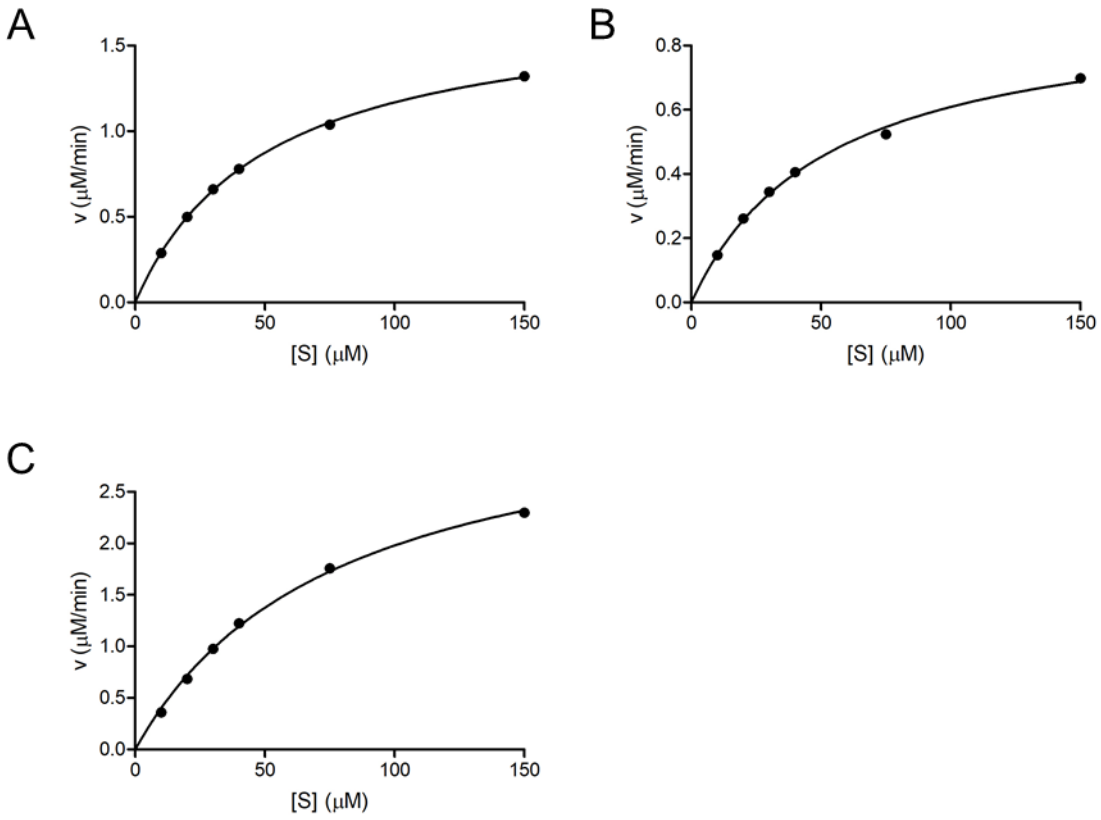

Figure 2-4. Dephosphorylation activity of WT PPM1A peptide substrates.

The velocity at each concentration of substrate is plotted. The data points were fitted to the Michaelis–Menten equation v = Vmax S/(K_m + S) by Prism5 software (Graph Pad Software). The activity for p38(180pT, 182pY) peptide (A), CaMKII peptide (B), and p53 peptide (C) is shown.

Table 2-3. Kinetic parameters of WT PPM1A for peptide substrates

Phosphopeptide	K_m (μM)	k_{cat} (s^{-1})	k_{cat}/K_m ($x10^4$, $s^{-1}M^{-1}$)
p38(180pT,182pY)	50.58	5.86	11.59
CaMKII(287pT)	52.52	3.10	5.90
p53(20pT)	78.14	11.80	15.10

Table 2-4. Dephosphorylation of PPM1A for peptide substrates

Dephosphorylation activity is shown as the turnover at a substrate concentration of 150 μM.

Phosphopeptide	PPM1A			
	WT	R33Q	R186Q	R33Q/R186Q
p38(180pT,182pY)	4.4	0.01	0.05	0.003
CaMKII(287pT)	2.33	0.22	0.31	0
p53(20pT)	7.66	0.38	0.11	0

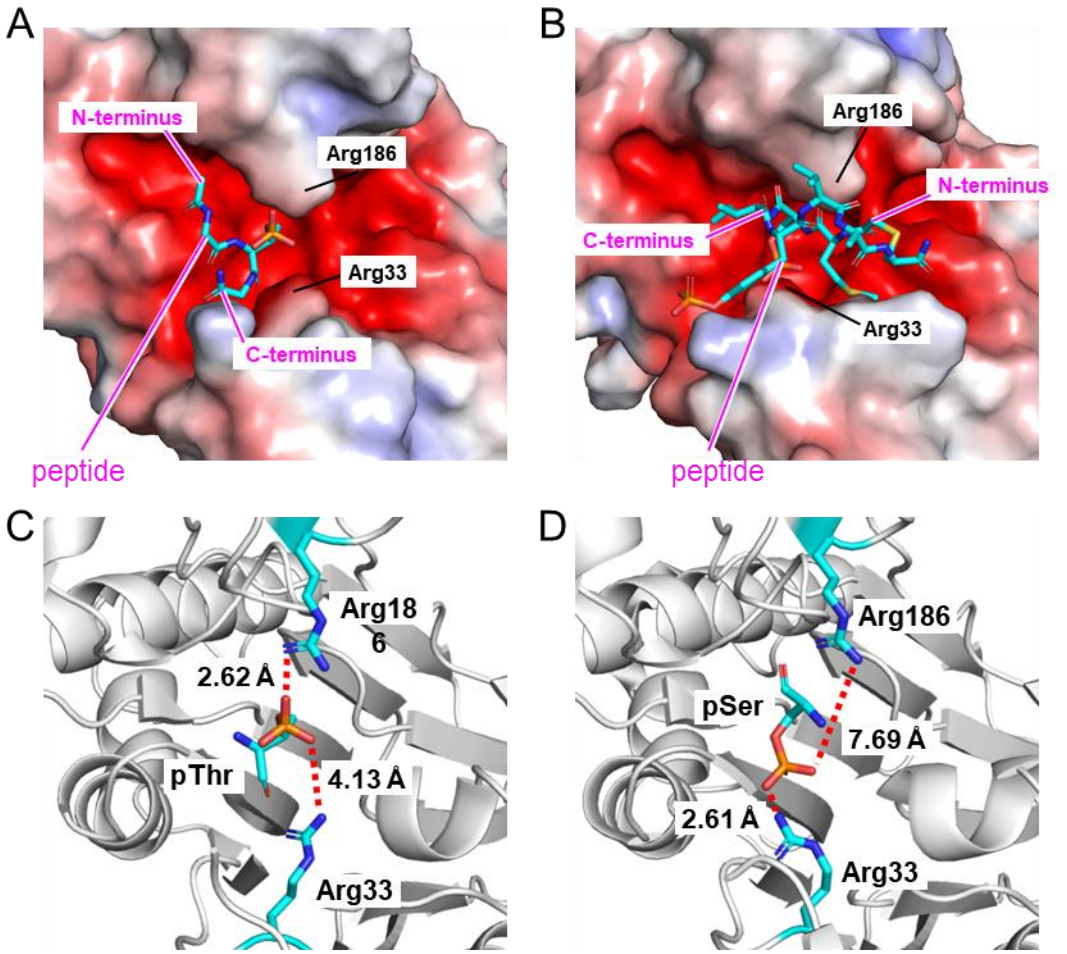

Figure 2-5. Distance from Arg33 and Arg186 to the substrate phosphate group.

(A) Docking model structure of the complex of PPM1A and Ac-Gly-pThr-Gly-NH_2 peptide. (B) Crystal structure of the D146E mutant PPM1A catalytic domain with a cyclic peptide, c(M(pS)I(pY)VA), which was designed according to the p38 sequence (PDB: 6B67). (C) The side chains of Arg33 and Arg186 from the docking model structure are shown with pThr of Ac-Gly-pThr-Gly-NH_2 peptide and a water molecule. (D) The side chains of Arg33 and Arg186 in the PPM1AcatD146E-c(M(pS)I(pY)VA) complex are shown with pSer of the cyclic peptide.

2.5 Discussion

pNPP showed much higher K_m and lower k_{cat}/K_m values than the model peptide, and only Arg33 was important for pNPP dephosphorylation. Therefore, we propose that pNPP, which is often used in the study of phosphatases, is not a good substrate of PPM.

R33Q and R186Q substitution significantly reduced the k_{cat}/K_m values for the model peptide compared with the WT. The effect of the decrease in the k_{cat} values was greater than the increase in the K_m values. It is possible that Arg33 and Arg186 interact with the phosphate group of the substrate and increase enzymatic turnover because the model peptide had no side chain adjacent to the phospho-Thr for the interaction with PPM1A.

In the dephosphorylation of the model peptide, Gln substitution at Arg186 reduced the k_{cat}/K_m value more significantly than Arg33. The phosphate group of the model peptide was positioned closer to Arg186 than Arg33. These results indicated that Arg186 had a more important role than Arg33 in the dephosphorylation of the model peptide. In the dephosphorylation of CaMKII and p53 peptide, the effect of Gln substitution at Arg33 or Arg186 were different, indicating that the contribution of the two Arg residues at the catalytic center differed for these peptides.

Both Arg33 and Arg186 are highly conserved in PPM1 isoforms (**Figure 2-6**). The residue corresponding to Arg33 in PPM1H, PPM1J, and PPM1M is Ser, and Arg33 is conserved in other isoforms. The residue corresponding to Arg186 in PPM1K is His, and Arg186 is conserved in other isoforms, showing that Arg186 is conserved more strictly than Arg33. These findings suggested that the interaction of Arg186 with the phosphate group of the substrate is a critical mechanism in substrate recognition. PPM1H, PPM1J, and PPM1M have basic residues adjacent to the position corresponding to Arg33 of PPM1A. It is possible that these basic residues contribute to the interaction with the phosphate group in PPM1H, PPM1J, and PPM1M.

Here, it was shown in the analysis using variants with Gln substitution that both Arg33 and Arg186

play important roles in the dephosphorylation of PPM1A via the interaction with the phosphate group of the substrate. It was suggested that the contribution of these two arginine residues to dephosphorylation is dependent on the sequence of the substrate. This provides new insights into the mechanism by which PPM1A recognizes the various sequences of the substrates.

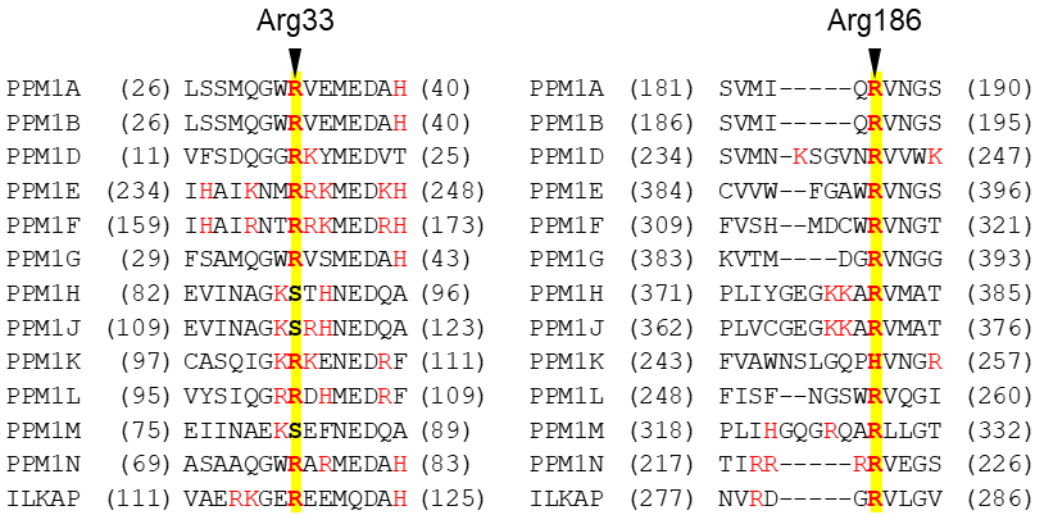

Figure 2-6. Sequence alignment of PPM1 isoforms.

Alignments were obtained using either the MEGA software or by visual inspection according to the crystal structure of PPM1A, PPM1B, and PPM1K. The residues corresponding to Arg33 and Arg186 in each PPM1 isoform are shown in bold and basic residues are colored.

2.6 References

1. Kamada, R., Kudoh, F., Ito, S., Tani, I., Janairo, J. I. B., Omichinski, J. G. & Sakaguchi, K. (2020) Metal-dependent Ser/Thr protein phosphatase PPM family: Evolution, structures, diseases and inhibitors. *Pharmacology & Therapeutics* **215**, 107622.
2. Tamura, S., Toriumi, S., Saito, J. I., Awano, K., Kudo, T. A. & Kobayashi, T. (2006) PP2C family members play key roles in regulation of cell survival and apoptosis. *Cancer Science* **97**, 563–567.
3. Shi, Y. (2009) Serine/Threonine Phosphatases: Mechanism through Structure. *Cell* **139**, 468–484.
4. Dvashi, Z., Shalom, H. S., Shohat, M., Ben-Meir, D., Ferber, S., Satchi-Fainaro, R., Ashery-Padan, R., Rosner, M., Solomon, A. S. & Lavi, S. (2014) Protein phosphatase magnesium dependent 1A governs the wound healing-inflammation-angiogenesis cross talk on injury. *American Journal of Pathology* **184**, 2936–2950.
5. Schaaf, K., Smith, S. R., Duverger, A., Wagner, F., Wolschendorf, F., Westfall, A. O., Kutsch, O. & Sun, J. (2017) Mycobacterium tuberculosis exploits the PPM1A signaling pathway to block host macrophage apoptosis. *Scientific Reports* **7**, 1–16.
6. Shohat, M., Ben-Meir, D. & Lavi, S. (2012) Protein phosphatase magnesium dependent 1A (PPM1A) plays a role in the differentiation and survival processes of nerve cells. *PLoS ONE* **7**, 1–11.
7. Mazumdar, A., Tahaney, W. M., Reddy Bollu, L., Poage, G., Hill, J., Zhang, Y., Mills, G. B. & Brown, P. H. (2019) The phosphatase PPM1A inhibits triple negative breast cancer growth by blocking cell cycle progression. *npj Breast Cancer* **5**, 1–11.
8. Fan, J., Yang, M. X., Ouyang, Q., Fu, D., Xu, Z., Liu, X., Mino-Kenudson, M., Geng, J. & Tang, F. (2016) Phosphatase PPM1A is a novel prognostic marker in pancreatic ductal

adenocarcinoma. *Human Pathology* **55**, 151–158.

9. Li, R., Gong, Z., Pan, C., Xie, D. D., Tang, J. Y., Cui, M., Xu, Y. F., Yao, W., Pang, Q., Xu, Z. G., Li, M. Y., Yu, X. & Sun, J. P. (2013) Metal-dependent protein phosphatase 1A functions as an extracellular signal-regulated kinase phosphatase. *FEBS Journal* **280**, 2700–2711.

10. Lin, X., Duan, X., Liang, Y. Y., Su, Y., Wrighton, K. H., Long, J., Hu, M., Davis, C. M., Wang, J., Brunicardi, F. C., Shi, Y., Chen, Y. G., Meng, A. & Feng, X. H. (2006) PPM1A Functions as a Smad Phosphatase to Terminate TGFβ Signaling. *Cell* **125**, 915–928.

11. Sun, W., Yu, Y., Dotti, G., Shen, T., Tan, X., Savoldo, B., Pass, A. K., Chu, M., Zhang, D., Lu, X., Fu, S., Lin, X. & Yang, J. (2009) PPM1A and PPM1B act as IKKβ phosphatases to terminate TNFα-induced IKKβ-NF-κB activation. *Cellular Signalling* **21**, 95–102.

12. Yamaguchi, H., Durell, S. R., Chatterjee, D. K., Anderson, C. W. & Appella, E. (2007) The Wip1 phosphatase PPM1D dephosphorylates SQ/TQ motifs in checkpoint substrates phosphorylated by PI3K-like kinases. *Biochemistry* **46**, 12594–12603.

13. Das, A. K., Helps, N. R., Cohen, P. T. & Barford, D. (1996) Crystal structure of the protein serine/threonine phosphatase 2C at 2.0 A resolution. *The EMBO Journal* **15**, 6798–6809.

14. Egloff, M. P., Cohen, P. T. W., Reinemer, P. & Barford, D. (1995) Crystal structure of the catalytic subunit of human protein phosphatase 1 and its complex with tungstate. *Journal of Molecular Biology* **254**, 942–959.

15. Lountos, G. T., Austin, B. P., Tropea, J. E. & Waugh, D. S. (2015) Structure of human dual-specificity phosphatase 7 , a potential cancer drug target research communications. 650–656 doi:10.1107/S2053230X1500504X.

16. Bobyr, E., Lassila, J. K., Wiersma-koch, H. I., Fenn, T. D., Lee, J. J., Nikolic-hughes, I., Hodgson, K. O., Rees, D. C., Hedman, B. & Herschlag, D. (2012) High-Resolution Analysis

of Zn 2 + Coordination in the Alkaline Phosphatase Superfamily by EXAFS and X-ray Crystallography. *Journal of Molecular Biology* **415**, 102–117.

17. Tanoue, K., Miller Jenkins, L. M., Durell, S. R., Debnath, S., Sakai, H., Tagad, H. D., Ishida, K., Appella, E. & Mazur, S. J. (2013) Binding of a third metal ion by the human phosphatases PP2C α and Wip1 is required for phosphatase activity. *Biochemistry* **52**, 5830–5843.

3. Development of the novel substrate identification method “Metal-dependent Substrate Trapping”

3.1 Abstract

Each PPM phosphatase isoform has varied and very important roles in cells, and the abnormal functions of PPMs cause many diseases such as cancer. However, little is known about their intracellular substrates. This is a large bottleneck for the elucidation of the cellular functions of PPM. To clarify the various functions of PPM, it is necessary to comprehensively identify the cellular substrates of PPM. In this study, we report the development of the novel substrate identification method “Metal-dependent Substrate Trapping” for wild-type PPM. This method is based on the novel principle that PPM activity is lost, while its ability to recognize substrates is retained by the replacement of Mg^{2+} with inactive divalent cations at the active center, resulting in the formation of stable enzyme–substrate complexes.

Here, it was shown that the substrates of PPM1A are specifically trapped by MdST with Zn^{2+}. Endogenous elongation factor 2 (eEF2), a reported substrate of PPM1A, was trapped by this method, indicating that this method is effective in identifying the cellular substrates of PPM. The nuclear lamina protein, lamin A/C, was identified by mass spectrometry as being among the proteins trapped by PPM1A. The phosphopeptides derived from lamin A/C were dephosphorylated by PPM1A, and the phosphorylation state of lamin C expressed in HeLa cells was altered by the expression of WT PPM1A. Therefore, we identified lamin A/C as a novel substrate of PPM1A. Thus, the MdST method may be quite an effective technique for discovering the cellular functions of PPM.

3.2 Introduction

PPMs are Mn^{2+}-/Mg^{2+}-dependent Ser/Thr phosphatases that have 20 isoforms in humans (1). Unlike other Ser/Thr phosphatases, PPM phosphatases do not require a regulatory subunit to recognize their substrates. The sequence of the catalytic domain and the metal chelating residues are highly conserved. The crystal structure of human PPM1A, PPM1B, and PPM1K have been reported and indicate that the 3D structure of the catalytic domain is highly conserved in PPM isoforms (2–4). The active center of PPM is negatively charged by conserved acidic residues, implying that the charge of the active center needs to be neutralized by the coordination of metal ions for the negatively charged substrate phosphate groups to be close to each other. Consequently, the coordination of divalent metal ions in the active center of PPM is important for substrate recognition. In addition, two Arg residues in the catalytic center of PPM1A interact with the substrate phosphate group, and the contribution of these Arg residues differs dependent on the substrate sequence. This provides new insights into the mechanism by which PPM1A recognizes a wide range of substrate sequences as a monomer. Because these Arg residues are highly conserved in other PPM isoforms, it is suggested that all PPM family members can recognize multiple substrate sequences.

PPM phosphatases are involved in various and important cellular processes such as proliferation, differentiation, immune response, and metabolism, and the abnormal functions of PPM cause many diseases including cancer (1,5). It is reported that PPM1A and ILKAP have tumor suppressor roles, whereas PPM1D functions in tumor progression (6–9). PPM1A is located in the nuclei and cytoplasm of cells, whereas PPM1L and PPM1K are localized in the ER and mitochondria. This indicates that each PPM family member has different roles in cells, suggesting that they dephosphorylate their specific substrates. However, little is known about the substrates of most PPM family members. In the study of signaling pathways that are activated by PPM, the identification of their substrates is a major bottleneck.

It is reported that the pT-X-pY motif is a substrate of PPM1A and PPM1D, and the pS/pT-Q motif is a substrate of PPM1D (10–12). However, PPM1A and PPM1D are known to dephosphorylate different

sequences to these motifs. There is no report on the substrate motifs of other PPM isoforms. Therefore, it is currently difficult to comprehensively search for substrate candidates by database analysis according to substrate motif.

Substrate-trapping methods using inactive mutants of the Tyr phosphatase PTP family and the Ser/Thr phosphatase PP1 family were reported as substrate identification methods for phosphatases (13–15). However, the active center of PPM is shallower than that of PTP and is involved in catalysis and substrate recognition, unlike PP1, which has a regulatory subunit to recognize its specific substrates. It is difficult to form PPM–substrate complexes with inactive mutants that change the structure and electric charge of the active center, and there has been no report on a substrate identification method for PPM phosphatase. Therefore, a substrate identification method for PPM phosphatase to detect the formation of stable complexes of PPM and substrate without changes in the electric charge and structure of the active center is required.

In this study, we report the development of a novel substrate identification method for wild-type PPM, "Metal-dependent Substrate Trapping" (MdST). In this method, Mn^{2+}/Mg^{2+} at the active center of PPM is replaced by an inactive divalent metal ion to inhibit its dephosphorylation activity and retain its ability to recognize specific substrates, resulting in the formation of stable PPM–substrate complexes. We show that the MdST method with Zn^{2+} is highly specific to the substrate sequence and can trap proteins from cell lysates using the active center of PPM1A. This method is an extremely effective method for comprehensively identifying the substrates of PPM, which have only been partially discovered to date.

3.3 Experimental procedures

3.3.1 Cell culture and materials

Human embryonic kidney 293 (HEK293) cells were obtained from ATCC (Rockville, MD) and HeLa cells were obtained from ATCC (Rockville, MD). Cells were cultured in Dulbecco's modified Eagles medium with 10% v/v fetal bovine serum, 100 units/mL penicillin, and 100 µg/mL streptomycin in a humidified atmosphere of 5% CO_2. Primary antibodies used were anti-eEF2 (#2332; Cell Signaling), anti-FLAG (F1804; Sigma–Aldrich), and anti-HA (H6908; Sigma–Aldrich). Secondary antibodies for western blotting and immunocytochemistry were anti-mouse IgG HRP (NA931V; GE Healthcare), anti-rabbit IgG HRP (7074S; Cell Signaling), Alexa fluor 488 goat anti-mouse IgG, and Alexa fluor 568 goat anti-rabbit IgG (both Invitrogen).

3.3.2 GST-PPM1A pull-downs of phosphopeptides

A premixed solution of H-eEF2(57pT), H-CaMKII(287pT), H-p38(180pT, 182pY), H-p38(180pT, 182Y), H-p38(180pS, 182pY), H-p53(15pS), and H-p53(315pS) was prepared in buffer (50 mM Tris HCl pH 7.5, 50 mM NaCl, and 0.1% TritonX-100). A total of 50 µL premixed solution was mixed with 50 µL Zn^{2+} solution (0.4 mM $ZnCl_2$, 50 mM Tris HCl pH 7.5, and 50 mM NaCl) followed by incubation with 5 µL glutathione Sepharose 4B beads that were fully occupied with GST-PPM1A for 1 h at 4°C. The beads were washed four times with 100 µL wash buffer (0.2 mM $ZnCl_2$, 50 mM Tris HCl pH 7.5, and 50 mM NaCl). Phosphopeptides trapped by PPM1A were eluted three times with 20 µL elution buffer (10 mM EDTA, 50 mM Tris HCl pH 7.5, and 50 mM NaCl). AcOH was added to the sample to a final concentration of 10%.

3.3.3 Metal-dependent Substrate Trapping in cell lysates

HEK293 cells were plated onto 10-cm dishes with 8 mL medium. Cell were washed with 5 mL cell wash buffer (50 mM Tris HCl pH 7.5, and 150 mM NaCl) and harvested from six confluent dishes with 900

μL lysis buffer. $ZnCl_2$ solution was added to the cell lysate to a final concentration of 0.2 mM and incubated for 1 h at 4°C. Ultracentrifugation was performed and the supernatant was mixed with 10 μL glutathione Sepharose 4B beads that were fully occupied with GST-PPM1A. After incubation for 1 h at 4°C, beads were washed five times with 200 μL beads wash buffer (50 mM Tris HCl pH 7.5, 150 mM NaCl, and 0.2 mM $ZnCl_2$). Proteins trapped by PPM1A were eluted with elution buffer (50 mM Tris HCl pH 7.5, 150 mM NaCl, and 10 mM EDTA). Depletion of the eluted samples was performed with 5 μL glutathione Sepharose 4B beads that were fully occupied with GST. The supernatant of the depleted samples was analyzed by hyper-sensitive CBB staining or nLC-MS/MS.

3.3.4 Western blotting analysis

MdST elute after depletion and cell lysates were mixed with 2× sample buffer (100 mM Tris-HCl pH6.8, 20% glycerol, 4% SDS, and 12% 2-mercaptoethanol). Proteins in these samples were separated by SDS-PAGE or Phos-tag SDS-PAGE, transferred to polyvinylidene difluoride membranes, and detected with the antibodies described above by enhanced chemiluminescence.

3.3.5 Immunocytochemistry

Cells were cultured on glass coverslips and fixed with 3.5% formalin/PBS at 15 min, washed with PBS three times, and treated with 0.2% TritonX-100/PBS. To suppress non-specific signals, cells were incubated with 10% FBS/PBS. Immunostaining was performed with the antibodies described above. Nuclei were stained with DAPI and cells were then observed by fluorescence microscopy (BZ-9000; Keyence).

3.4 Results

3.4.1 Effect of divalent metal ions on PPM1A activity

To examine the effect of Mn^{2+} and Mg^{2+} on the activation of PPM1A, *in vitro* phosphatase assay was performed in the presence of Mn^{2+} or Mg^{2+}. In the dephosphorylation of eEF2(57pT) and p38(180pT, 182Y), Mg^{2+} activated PPM1A more significantly than Mn^{2+} (**Figure 3-1**). The effect of stable 4th period divalent metal ions (Ca^{2+}, Co^{2+}, Ni^{2+}, Zn^{2+}) on PPM1A activation by Mg^{2+} was analyzed. In conditions of sufficiently high concentrations of phosphopeptide substrate p38(180pT, 182pY), 0.2 mM Zn^{2+} completely inhibited the activation of PPM1A by 30 mM Mg^{2+} (**Figure 3-2A**). Furthermore, 0.2 mM Ca^{2+} had no effect on PPM1A activity. In addition, 0.2 mM Co^{2+} and 0.2 mM Ni^{2+} reduced PPM1A activity to 88.6% and 71.3%, respectively, indicating that the inhibition by Co^{2+} and Ni^{2+} was weaker than that of Zn^{2+}. To examine the inhibition mode of Zn^{2+}, which showed the strongest inhibition on PPM1A activity, PPM1A activity with 2–10 mM Mg^{2+} in the presence of Zn^{2+} was evaluated. This showed that Zn^{2+} competitively inhibited PPM1A and that the Ki value was 13.25 nM. These results demonstrated that Mg^{2+} ions in the active center of PPM1A were replaced by Zn^{2+}, resulting in the inactivation of PPM1A. To analyze the effect of Zn^{2+} coordination at the active center of the PPM1A structure, CD spectra in the presence of Zn^{2+} were measured. The results showed that CD in the presence of Zn^{2+} was almost same as the CD without Zn^{2+}, indicating that the coordination of Zn^{2+} at the active center did not change the PPM1A structure (**Figure 3-3**). Therefore, the structure and charge of the active center of PPM1A inactivated by Zn^{2+} were likely to be close to that of the active PPM1A with Mg^{2+}, and that PPM1A bound to Zn^{2+} recognized the native substrate and formed a complex with the substrate. Here, we designed a novel substrate identification method, the MdST method, in which the substrate was identified by purifying the complex of PPM1A inactivated by Zn^{2+} and the substrates derived from the cell lysates. PPM phosphatase activated by Mg^{2+} recognizes its substrate and releases the dephosphorylated product. However, in the MdST method, PPM phosphatase inactivated by Zn^{2+} retains the ability to recognize the substrate, resulting in the formation of stable complexes with the substrates (**Figure**

3-4).

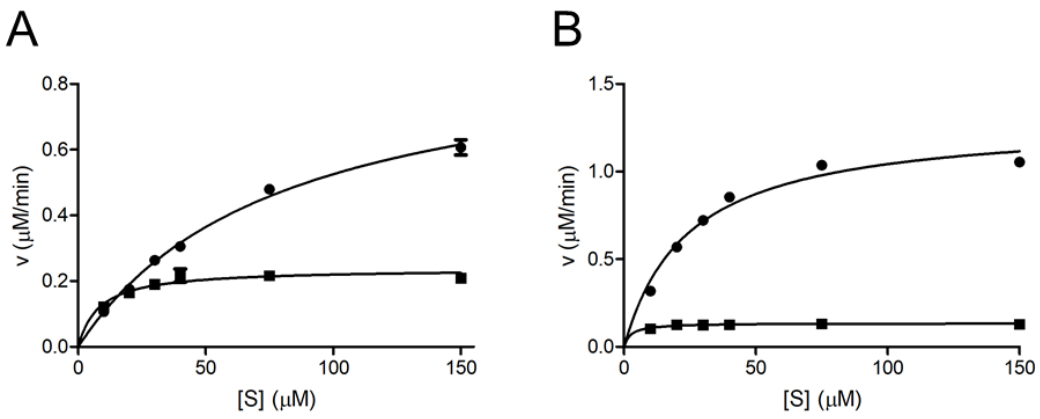

Figure 3-1. Effect of Mn^{2+} and Mg^{2+} on the activation of PPM1A.

The catalytic activity of PPMM1A was measured with (A) H-eEF2(62–64:57pT) and (B) H-p38(176–186:180pT, 182Y). The activity with 10 mM Mn^{2+} is shown as squares, and the activity with 30 mM Mg^{2+} is shown as circles. Experiments were performed in 50 mM Tris HCl pH 7.4, 0.02% 2-mercaptoethanol, and 0.1 mM EGTA at 30°C with 10–150 μM peptide. The data points were fitted to the Michaelis–Menten equation v = Vmax S/(K_m + S) by Prism5 software (Graph Pad Software).

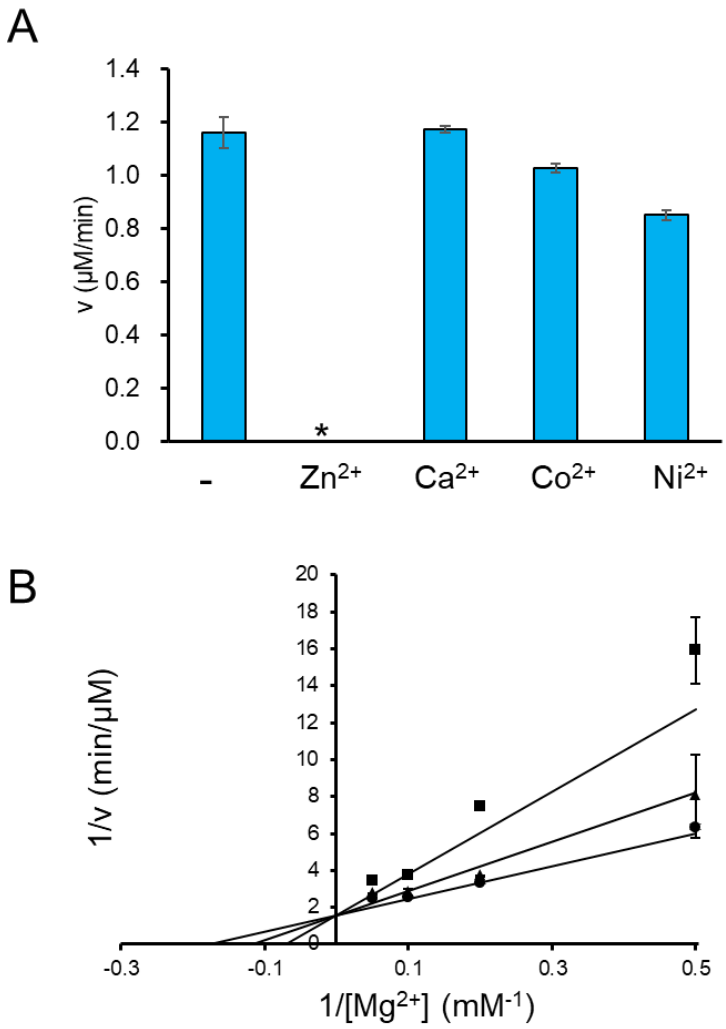

Figure 3-2. Inhibition of PPM1A activity by divalent metal ions.

(A) The catalytic activity of PPM1A for H-p38(176–186: 180pT, 182pY) was measured at a substrate concentration of 150 μM with 30 mM Mg^{2+} and 0.2 mM of each metal ion. Experiments were performed in 50 mM Tris HCl pH 7.4, 0.02% 2-mercaptoethanol, and 0.1 mM EGTA at 30°C. (B) Double-reciprocal plot (1/v vs. 1/(Mg^{2+}]) of the effect of Zn^{2+} on PPM1A activity for H-p38(176–186: 180pT, 182Y). Zn^{2+} was the inhibitor (0, 10, and 30 nM are shown as circles, triangles, and squares, respectively), and Mg^{2+} was the variable substrate. Experiments were performed in 50 mM Tris HCl pH 7.4. The Ki value was determined by global fitting with Prism5 software (Graph Pad Software).

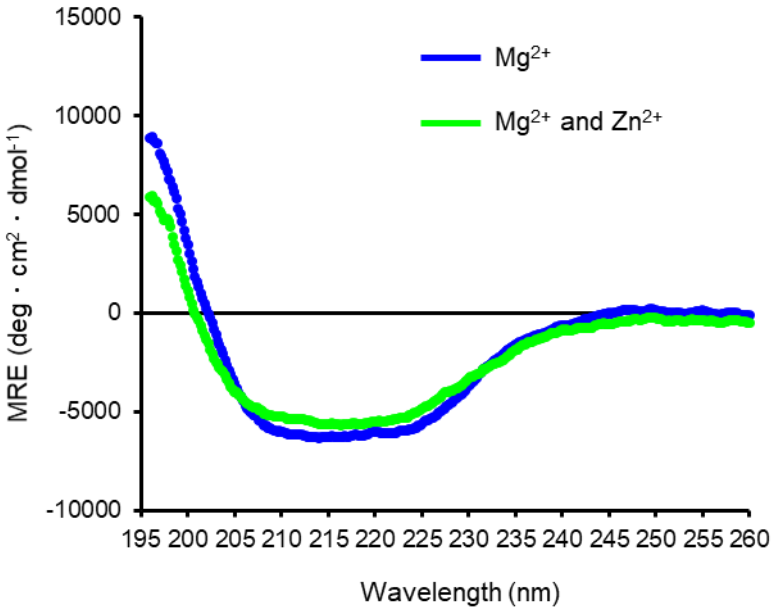

Figure 3-3. CD spectra of PPM1A in the presence of Mg^{2+} and/or Zn^{2+}.

Spectra for 0 mM Mg^{2+} (blue), 5 μM Zn^{2+} (red), and 10 mM Mg^{2+} and 5 μM Zn^{2+} (green) are shown.

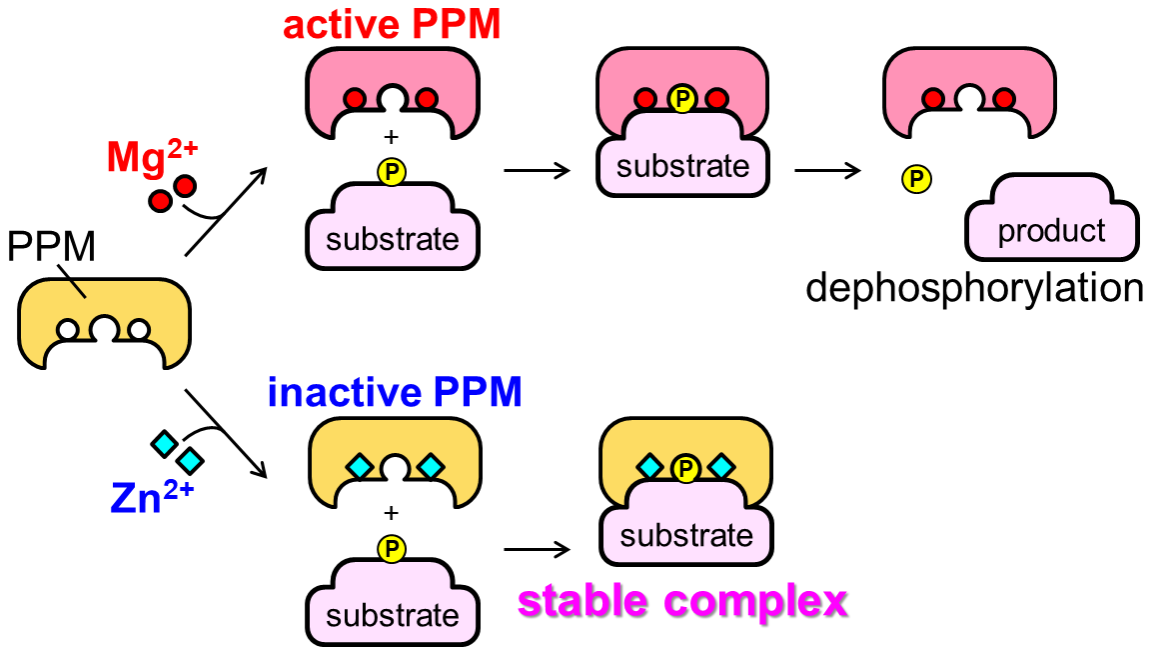

Figure 3-4. Schematic of the Metal-dependent Substrate Trapping model.

PPM phosphatase recognizes its substrate and releases the dephosphorylated product in the presence of Mg^{2+}. PPM phosphatase bound to inactivating metal ions loses its activity but retains the ability to recognize the substrate, resulting in the formation of stable complexes with its substrates.

3.4.2 Target-specific binding of MdST with Zn^{2+}

The K_m value of PPM1A for H-p38(180pT, 182pY) and H-p38(180pT, 182Y) was 80.51 μM and 24.32 μM, respectively. Substitution of Tyr for phospho-Tyr in H-p38(180pT, 182pY) peptide decreased the K_m value, as previously reported (K_m: 63 μM for p38(180pT, 182pY). The kinetic parameters of H-p38(180pS, 182pY) could not be determined due to the high K_m. These results suggested that H-p38(180pT, 182Y) had the highest affinity to PPM1A among these p38 peptides, while H-p38(180pS, 182pY) had the lowest affinity. The K_m value for H-CaMKII(287pT) was 1.4-fold lower than for H-p38(180pT, 182pY). The K_m and k_{cat} values of H-p53(315pS) could not be determined because of the low activity even at a substrate concentration of 150 μM (**Figure 3-5, Table 3-1**). GST-PPM1A pull-downs for the mixture containing H-CaMKII(287pT), H-p38(180pT, 182pY), H-p38(180pT, 182Y), H-p38(180pS, 182pY), and H-p53(315pS) were performed in the presence of Zn^{2+}. Standard curves of the intensity of nLC-MS/MS against the amount of each peptide trapped by PPM1A were obtained (**Figure 3-6**). The peptides trapped by PPM1A were quantified with these standard curves (**Table 3-2**). It was shown that H-CaMKII(287pT), H-p38(180pT, 182pY), H-p38(180pT, 182pY), and H-p38(180pS, 182pY) were trapped by PPM1A 17–163 times more than H-p53(315pS). Although the dephosphorylation activity of PPM1A for H-p38(180pS, 182pY) was low, H-p38(180pS, 182pY) was pulled down by PPM1A to almost the same amount as H-p38(180pT, 182pY). These results showed that MdST with Zn^{2+} is highly specific to the substrate sequence. The crystal structure of AgaP, the PPM phosphatase of *Anopheles gambiae*, has been reported in a bound state with Zn^{2+}. The homology model structure of PPM1A constructed using the AgaP crystal structure as the template was prepared. The overall crystal structure and homology model of PPM1A were the same (**Figure 3-7A**). The homology model of AgaP constructed using PPM1A crystal structure as the template was the same as the AgaP crystal structure (**Figure 3-7B**). In addition, the positions of the Asp side chains of the active center of PPM1A and AgaP were found to be in the same position as the Asp side chains in their homology model structures (**Figure 3-7C, D**). These findings suggest that the Mg^{2+} in the PPM1A active center was replaced by Zn^{2+} and that the overall

structure and Asp position of PPM1A remained unchanged. It was shown that PPM1A was inactivated by the replacement of Mn^{2+}/Mg^{2+} with Zn^{2+} at the active center and that the replacement did not change the PPM1A structure.

Avidin-biotinylated peptide complex was prepared as a mimic of the substrate protein. GST-PPM1A pull-down for avidin-biotinylated peptide complexes was performed in the presence of Zn^{2+} (**Figure 3-8A**). The complex trapped by PPM1A was eluted by EDTA and detected by silver staining. The complex with CaMKII(287pT) peptide, which was dephosphorylated by PPM1A, was trapped more than the complex with p53(15pS) or p53(315pS) (**Figure 3-8B**). These results showed that the substrate proteins can be trapped by MdST with Zn^{2+}.

3.4.3 Pull-down of the cellular substrate of PPM1A

To confirm that cellular proteins were specifically trapped by the MdST method, GST-PPM1A pull-down of lysates from HEK293 cells was performed. The proteins bound to the catalytic center of PPM1A in a Zn^{2+}-dependent manner were eluted by EDTA. Non-specific proteins were removed by depletion with glutathione beads occupied by GST. Phos-tag SDS-PAGE for cells stimulated by nocodazole and western blotting with anti-eEF2 antibody showed that eEF2 was phosphorylated in cells and that the phosphorylation of eEF2 was decreased (**Figure 3-9A**). Western blotting with anti-eEF2 antibody for proteins trapped by the MdST method clearly showed that eEF2 was specifically trapped by PPM1A in the presence of Zn^{2+} (**Figure 3-9B**). In the silver-stained gel, PPM1A-specific bands were observed when the pull-down was performed with Zn^{2+}, whereas these PPM1A-specific bands were not observed when the pull-down was performed with Mn^{2+} or Ca^{2+} (**Figure 3-10A and B**). These results showed that the MdST method is Zn^{2+}-dependent and that the endogenous cellular substrates of PPM1A can be trapped by this method.

3.4.4 Identification of candidate novel cellular substrates of PPM1A

To identify the novel substrates of PPM1A, MdST with Zn^{2+} for lysates from HEK293 cells was

performed and the sample was analyzed by hyper-sensitive CBB staining. Because the detection sensitivity of hyper-sensitive CBB is lower than that of silver staining, the bands observed in **Figure 11** were fewer than those in **Figure 10A** but the pattern of the bands was the same. PPM1A-specific bands, bands A–C (indicated by arrow heads), were trypsinized and analyzed by nLC-MS/MS. In addition, bands D and E found in both PPM1A and GST were also analyzed by nLC-MS/MS. In each band, several proteins were identified. Forty proteins were listed in the order of the nLC-MS/MS score, which indicated the confidence of the identification (**Tables 3-3 – 3-7**). For band B, which showed the strongest signal by CBB staining, PPM1A was detected as the protein with the highest score, suggesting that part of GST-PPM1A for MdST was eluted (**Table 3-4**). In bands B and C, lamin A and lamin C, the splice variants encoded by *LMNA* gene, were identified as the proteins with the highest scores (**Table 3-3, 3-5**). In bands D and E, α-actin was identified as the protein with the highest score, indicating that band D was mainly non-specific protein. However, eEF2, the reported substrate of PPM1A, was detected only in band D, but not in band E (**Table 3-6, 3-7**). This result showed that substrates of PPM1A can be identified by this in-gel digestion method. The shotgun method for MdST samples was performed, and lamin A/C was detected as having the highest score with a coverage of 94% (**Table 3-8**). PPM1A was identified as the second highest scoring protein, suggesting that GST-PPM1A used for MdST was also detected by the shotgun method. Cortactin was detected as the third highest scoring protein. Cortactin was also detected in band A by in-gel digestion (**Table 3-3**). In addition, eEF2 was also detected by the shotgun method (**Table 3-8**). Eight phospho-Ser/Thr sites in lamin A/C and six phospho-Ser/Thr sites in cortactin were detected by the shotgun method (**Figure 3-12, 3-13**). In summary, phosphorylated substrates are trapped by the MdST method in principle. Therefore, it is possible that these phospho-Ser/Thr residues are substrates of PPM1A.

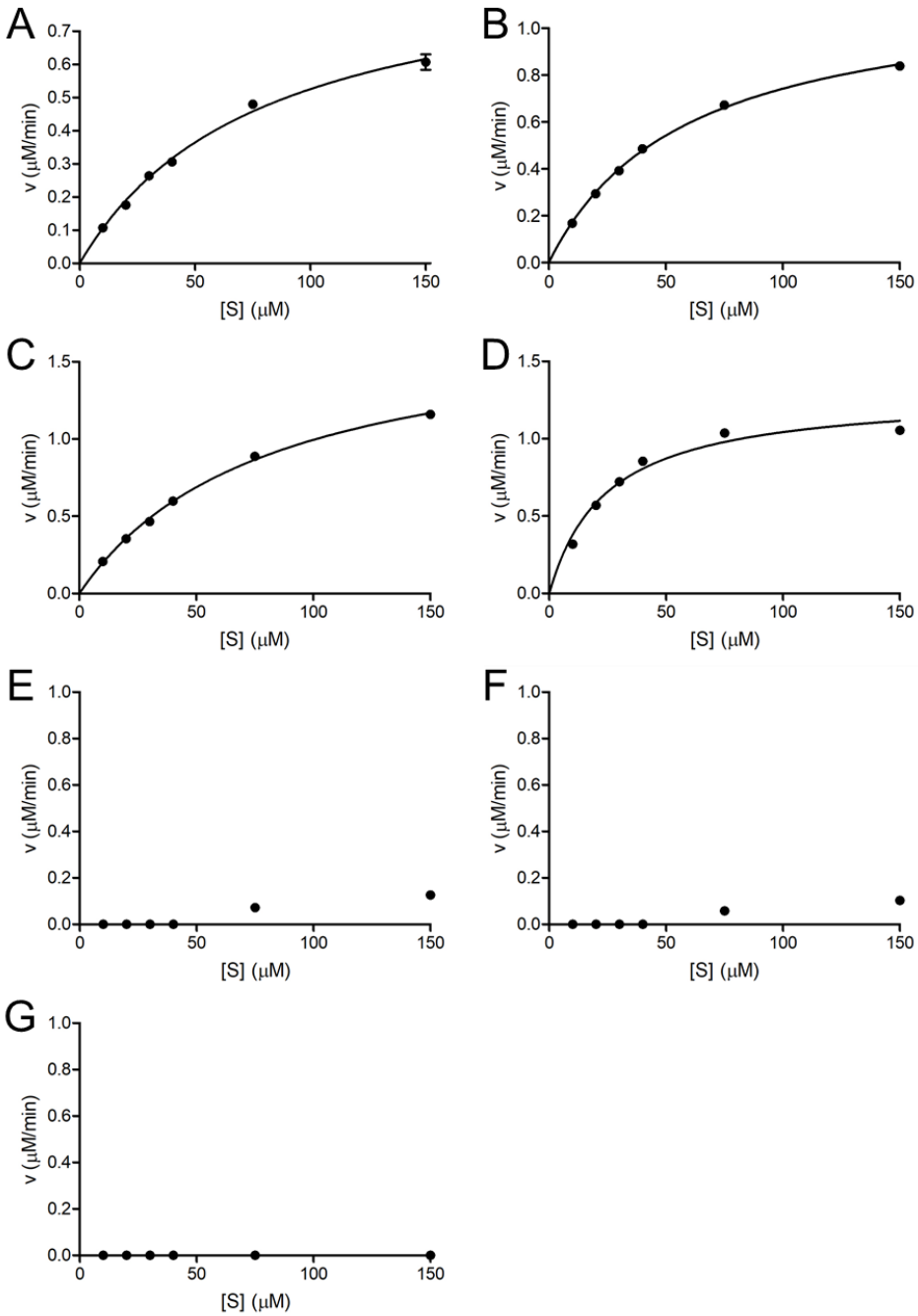

Figure 3-5 PPM1A dephosphorylation activity of phosphopeptides.

Catalytic activity was measured with (A) H-eEF2(62–64: 57pT), (B) H-CaMKIIg(287pT), (C) H-p38(176–186: 180pT, 182pY), (D) H-p38(176–186: 180pT, 182Y), (E) H-p38(176–186: 180pS, 182pY), (F) H-p53(15pS), and (G) H-p53(315pS). Experiments were performed in 50 mM Tris HCl pH 7.4, 30 mM $MgCl_2$, 0.02% 2-mercaptoethanol, and 0.1 mM EGTA at 30°C. The data points were fitted to the Michaelis–Menten equation $v = V_{max}\, S/(K_m + S)$ by Prism5 software (Graph Pad Software). (A) and (C) are the same data as the plots with Mg^{2+} of Figure 1A and B, respectively.

Table 3-1. Kinetic parameters of the dephosphorylation activity of PPM1A for phosphopeptides

peptide	sequence	K_m (μM)	k_{cat} (s^{-1})	k_{cat}/K_m ($x10^4, s^{-1}M^{-1}$)
H-eEF2(52-64:57pT)	H-WG-GETRF(pT)DTRKDEQ-NH_2	78.88	3.13	3.97
H-CaMKII(282-292:287pT)	H-WG(Nle)HRQE(pT)VE(Abu)LR-NH_2	58.34	3.92	6.72
H-p38(176-186:180pT,182pY)	H-DDE(Nle)(pT)G(pY)VATR-NH_2	80.51	5.98	7.43
H-p38(176-186:180pT,180Y)	H-DDE(Nle)(pT)GYVATR-NH_2	24.32	4.32	17.76
H-p38(176-186:180pS,182pY)	H-DDE(Nle)(pS)G(pY)VATR-NH_2	NA[a]	NA[a]	NA[a]
H-p53(10-24:15pS)	H-VEPPL(pS)QETFSDLWK-NH_2	NA[a]	NA[a]	NA[a]
H-p53(309-323:315pS)	H-WNNTSS(pS)PQPKKKPL-NH_2	NA[a]	NA[a]	NA[a]

[a] NA, not active. Unable to determine kinetic parameters.

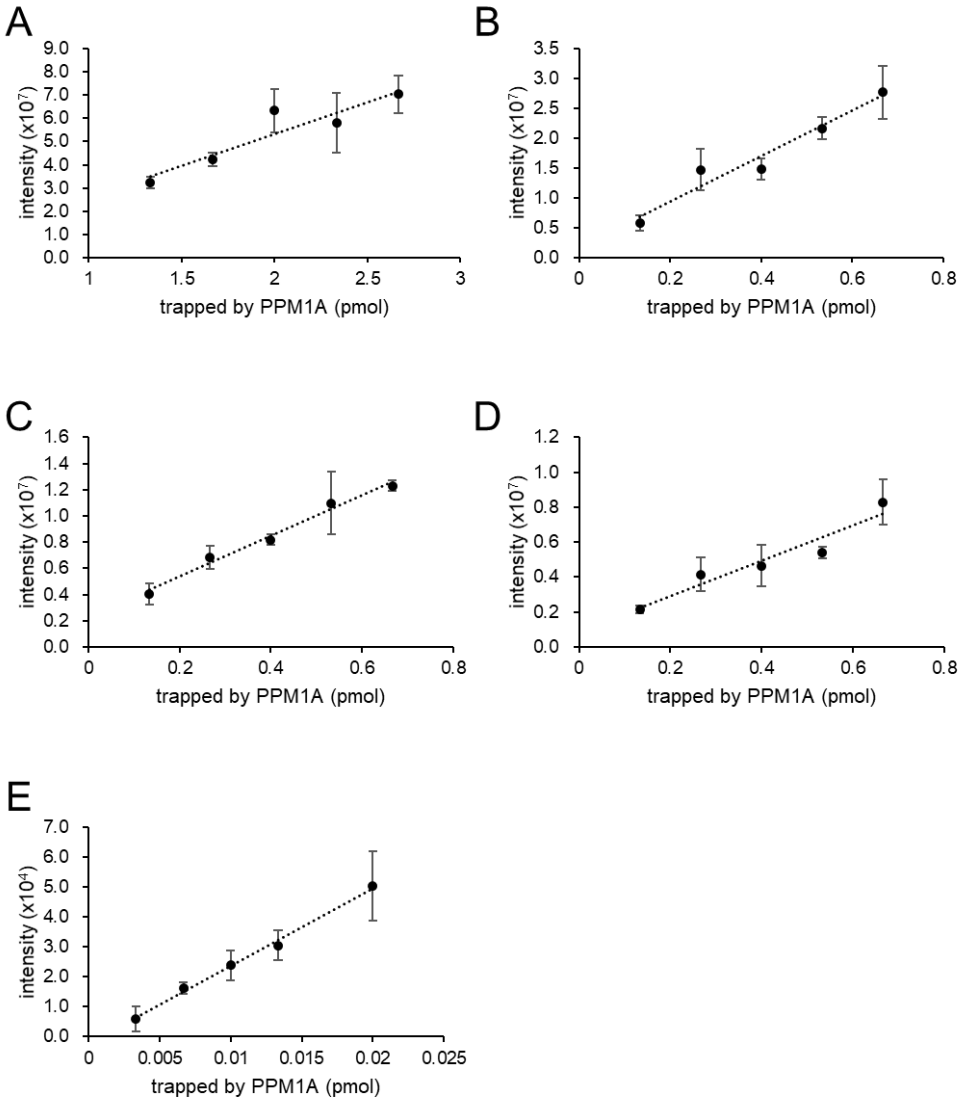

Figure 3-6. Standard curves for nLC-MS/MS intensity of phosphopeptides.

The standard curves of (A) H-CaMKII(287pT), (B) H-p38(176-186:180pT, 182pY), (C) H-p38(176–186:180pT, 182Y), (D) H-p38(176–186:180pS, 182pY), and (E) H-p53(315pS) are shown.

Table 3-2. GST-PPM1A pull-down of phosphopeptides

Phosphopeptides trapped by PPM1A in the presence of Zn^{2+} were quantified by nLC-MS/MS intensity and standard curves

peptide	sequence	trapped (pmol)
H-CaMKII(282-292:287pT)	H-WG(Nle)HRQE(pT)VE(Abu)LR-NH_2	1.47 ± 0.98
H-p38(176-186:180pT,182pY)	H-DDE(Nle)(pT)G(pY)VATR-NH_2	0.192 ± 0.033
H-p38(176-186:180pT,180Y)	H-DDE(Nle)(pT)GYVATR-NH_2	0.303 ± 0.014
H-p38(176-186:180pS,182pY)	H-DDE(Nle)(pS)G(pY)VATR-NH_2	0.153 ± 0.017
H-p53(309-323:315pS)	H-WNNTSS(pS)PQPKKKPL-NH_2	0.009 ± 0.0006

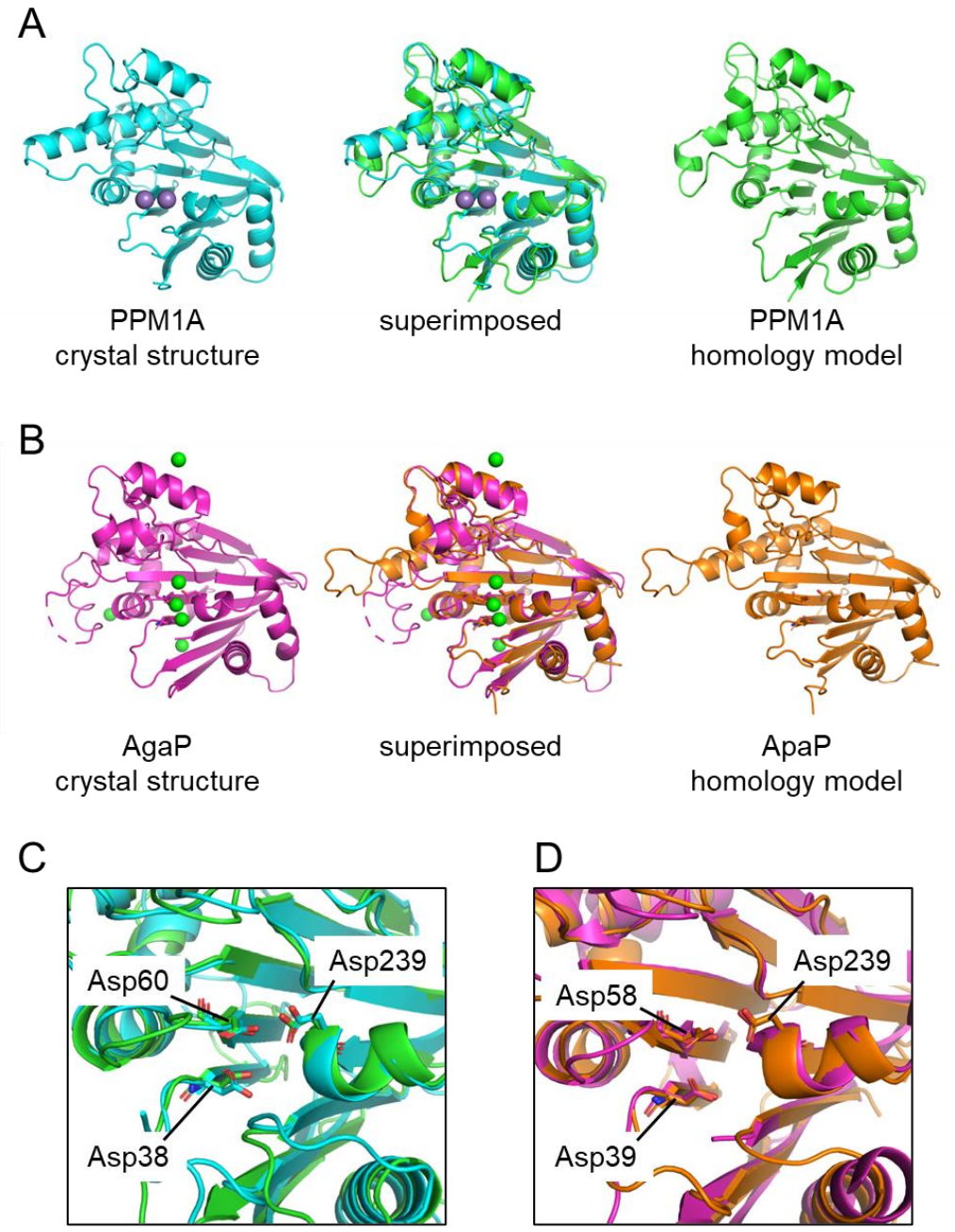

Figure 3-7. Three-dimensional structure of PPM1A and AgaP.
(A) Crystal structure of human PPM1A with Mn^{2+} (PDB ID: 1A6Q) and a homology model structure of PPM1A constructed using the crystal structure of Zn^{2+}-bound AgaP (PDB ID: 2I0O) as a template. Mn^{2+} is indicated by gray balls. (B) Crystal structure of human AgaP with Zn^{2+} (PDB ID: 2I0O) and a homology model structure of AgaP constructed using the crystal structure of Mn^{2+}-bound PPM1A (PDB ID: 1A6Q) as a template. Zn^{2+} is indicated by green balls. The active center of the super imposed structure of PPM1A (C) and AgaP (D).

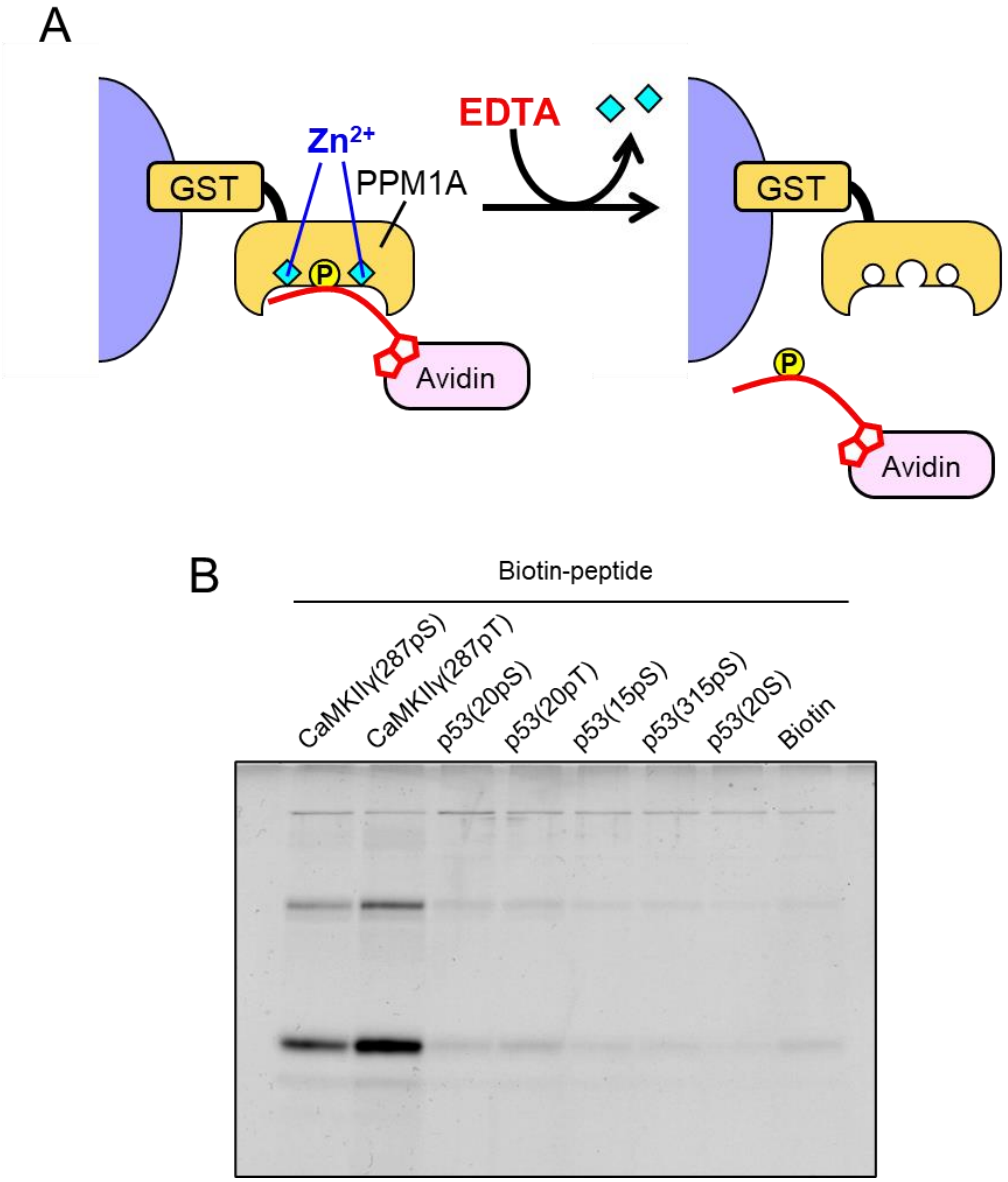

Figure 3-8. GST-PPM1A pull-down with Zn^{2+} for avidin-biotinylated peptide complexes

(A) Schematic of GST-PPM1A pull-down of the complexes. (B) Avidin protein eluted by EDTA was detected by silver staining.

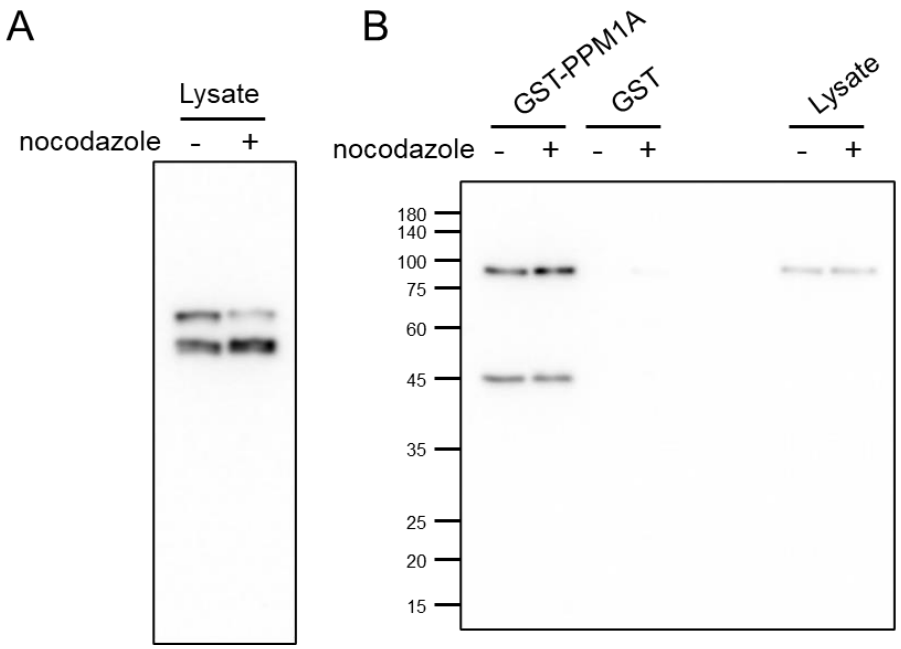

Figure 3-9. PPM1A-specific trapping of the reported substrate, eEF2.

(A) Phos-tag SDS-PAGE for HEK293 cell lysates. Western blotting was performed with anti-eEF2 antibody.

(B) SDS-PAGE and western blotting was performed with anti-eEF2 antibody for the MdST samples.

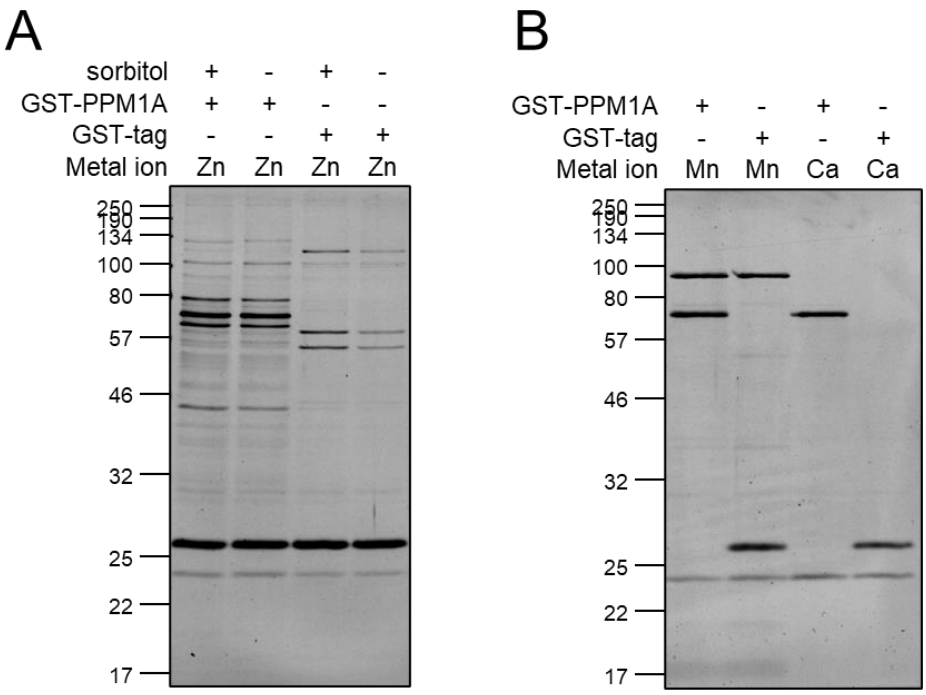

Figure 3-10. Zn^{2+}-dependent trapping of cellular proteins.

MdST experiments were performed with Zn^{2+}, Mn^{2+}, and Ca^{2+}. Trapped proteins were analyzed by silver staining.

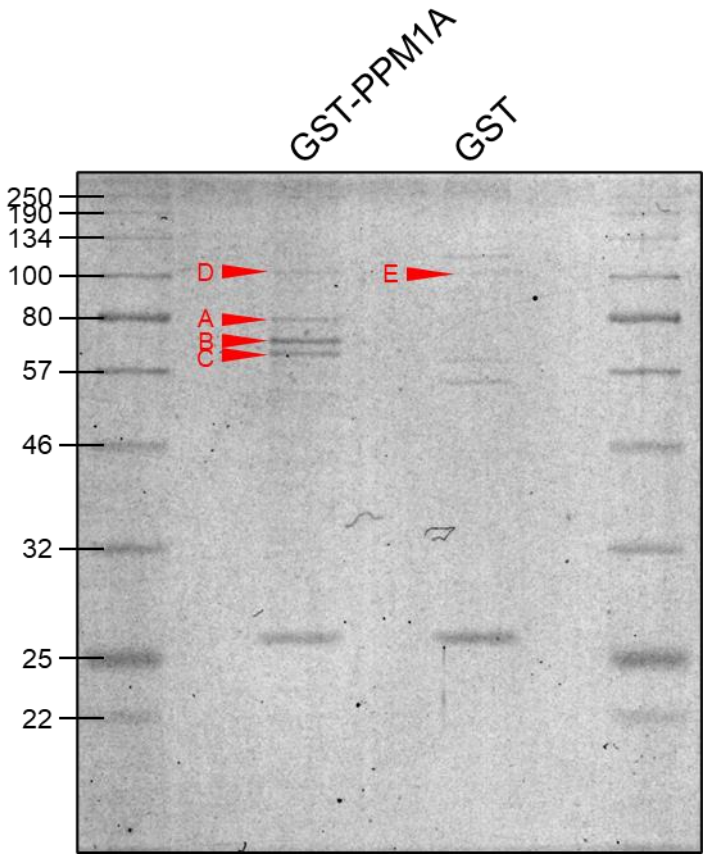

Figure 3-11. Hyper-sensitive CBB staining for MdST samples.

In-gel digestion and nLC-MS/MS analysis were performed for the bands indicated by arrow heads.

Table 3-3. nLC-MS/MS-detected proteins in band A (top 30)

Protein	Score	Coverage
Prelamin-A/C	372.95	63.86
Isoform ADelta10 of Prelamin-A/C	355.54	64.51
Isoform 6 of Prelamin-A/C	346.39	61.89
Isoform C of Prelamin-A/C	334.67	64.16
Isoform 5 of Prelamin-A/C	308.62	64.25
Isoform 4 of Prelamin-A/C	308.62	63.24
Endoplasmic reticulum chaperone BiP	86.17	35.17
Src substrate cortactin	76.13	37.09
Keratin, type II cytoskeletal 1	75.57	24.69
Isoform 3 of Src substrate cortactin	70.31	35.87
Isoform 2 of Src substrate cortactin	66.81	27.13
Keratin, type I cytoskeletal 10	61.90	20.03
Keratin, type II cytoskeletal 2 epidermal	50.82	25.20
BAG family molecular chaperone regulator 3	39.87	32.17
Septin-9	31.03	16.89
Isoform 2 of Septin-9	31.03	17.43
Isoform 5 of Septin-9	31.03	17.10
Isoform 7 of Septin-9	31.03	17.46
Isoform 3 of Septin-9	20.82	17.06
Alpha-actinin-1	15.89	5.72
Alpha-actinin-4	15.89	5.60
Isoform 4 of Alpha-actinin-1	15.89	5.48
Isoform 2 of Alpha-actinin-1	15.89	5.75
Isoform 3 of Alpha-actinin-1	15.89	5.58
Isoform 4 of Septin-9	12.07	12.54
Isoform 8 of Septin-9	12.07	8.86
Isoform 9 of Septin-9	12.07	11.60
Isoform ACTN4ISO of Alpha-actinin-4	11.88	5.64
Keratin, type II cytoskeletal 6B	11.80	5.14
Keratin, type I cytoskeletal 14	11.24	3.81

Table 3-4. nLC-MS/MS-detected proteins in band B (top 30)

Protein	Score	Coverage
Protein phosphatase 1A	424.70	79.84
Isoform 3 of Protein phosphatase 1A	424.70	67.03
Isoform Alpha-2 of Protein phosphatase 1A	308.02	75.31
PDZ and LIM domain protein 5	180.34	47.82
Isoform 7 of PDZ and LIM domain protein 5	151.88	42.44
Isoform 4 of PDZ and LIM domain protein 5	151.88	42.09
Isoform 6 of PDZ and LIM domain protein 5	132.61	29.76
Keratin, type II cytoskeletal 1	88.57	31.52
Lamin-B1	85.00	33.62
Keratin, type II cytoskeletal 2 epidermal	76.76	22.38
Heat shock cognate 71 kDa protein	73.61	29.41
Prelamin-A/C	70.33	27.56
Isoform C of Prelamin-A/C	70.33	31.99
Isoform 6 of Prelamin-A/C	70.33	29.80
Keratin, type I cytoskeletal 10	69.65	25.68
Src substrate cortactin	66.47	27.27
Isoform 3 of Src substrate cortactin	66.47	27.88
Isoform ADelta10 of Prelamin-A/C	65.85	26.66
Isoform 2 of Heat shock cognate 71 kDa protein	61.49	30.02
Isoform 3 of PDZ and LIM domain protein 5	61.33	51.87
Lamin B1, isoform CRA_a	61.15	47.72
Isoform 2 of Src substrate cortactin	59.46	20.66
Isoform 2 of PDZ and LIM domain protein 5	58.68	41.45
Protein phosphatase 1B	57.98	6.89
Isoform Beta-2 of Protein phosphatase 1B	57.98	8.53
Isoform 4 of Protein phosphatase 1B	57.98	8.68
Isoform 5 of Protein phosphatase 1B	57.98	10.09
Uncharacterized protein	57.98	8.59
Isoform 5 of Prelamin-A/C	48.08	24.07
Isoform 4 of Prelamin-A/C	48.08	23.69

Table 3-5. nLC-MS/MS-detected proteins in band C (top 30)

Protein	Score	Coverage
Isoform C of Prelamin-A/C	466.36	77.62
Prelamin-A/C	444.90	62.95
Isoform 6 of Prelamin-A/C	444.90	68.08
Isoform ADelta10 of Prelamin-A/C	418.59	63.56
Isoform 5 of Prelamin-A/C	344.90	58.76
Isoform 4 of Prelamin-A/C	344.90	57.84
Keratin, type II cytoskeletal 1	279.24	54.97
Protein phosphatase 1A	197.50	63.09
Isoform 3 of Protein phosphatase 1A	197.50	52.97
Keratin, type I cytoskeletal 10	192.39	58.56
Isoform Alpha-2 of Protein phosphatase 1A	156.58	61.11
Keratin, type II cytoskeletal 2 epidermal	145.08	51.49
Stress-induced-phosphoprotein 1	143.60	44.75
Isoform 2 of Stress-induced-phosphoprotein 1	143.60	41.19
Isoform 3 of Stress-induced-phosphoprotein 1	130.39	45.47
Keratin, type I cytoskeletal 9	79.01	26.97
Paraspeckle component 1	55.96	24.47
PDZ and LIM domain protein 5	53.10	34.56
Isoform 2 of Paraspeckle component 1	46.19	25.70
Keratin, type II cytoskeletal 5	34.77	15.59
Isoform 7 of PDZ and LIM domain protein 5	32.42	27.54
Isoform 4 of PDZ and LIM domain protein 5	32.42	27.31
Isoform 6 of PDZ and LIM domain protein 5	27.32	18.24
Keratin, type I cytoskeletal 14	24.50	13.14
Keratin, type II cytoskeletal 6B	23.96	10.11
Keratin, type II cytoskeletal 2 oral	23.51	7.37
Keratin, type I cytoskeletal 16	21.97	10.99
Protein phosphatase 1B	21.68	6.47
Isoform Beta-2 of Protein phosphatase 1B	21.68	8.01
Isoform 4 of Protein phosphatase 1B	21.68	8.16

Table 3-6. nLC-MS/MS-detected proteins in band D (top 30)

Protein	Score	Coverage
Alpha-actinin-4	406.57	72.34
Isoform ACTN4ISO of Alpha-actinin-4	299.07	68.35
Alpha-actinin-1	251.95	57.06
Isoform 3 of Alpha-actinin-1	251.95	55.69
Isoform 2 of Alpha-actinin-1	237.61	55.13
Isoform 4 of Alpha-actinin-1	230.86	50.97
Isoform 3 of Alpha-actinin-4	219.77	66.03
Alpha-actinin-2	105.53	16.44
Isoform 2 of Alpha-actinin-2	105.53	16.44
Splicing factor, proline- and glutamine-rich	95.55	28.85
Keratin, type II cytoskeletal 1	92.52	24.53
Isoform Short of Splicing factor, proline- and glutamine-rich	82.10	26.46
Targeting protein for Xklp2	64.96	27.98
Keratin, type II cytoskeletal 2 epidermal	59.76	23.47
Isoform 2 of Targeting protein for Xklp2	57.46	23.63
Keratin, type I cytoskeletal 10	53.34	24.32
Alpha-actinin-3	52.02	11.54
Elongation factor 2	38.75	15.73
DNA replication licensing factor MCM3	22.04	10.27
Isoform 2 of DNA replication licensing factor MCM3	22.04	9.73
Serum albumin	18.12	4.43
Albumin, isoform CRA_k	18.12	6.47
Isoform 2 of Serum albumin	18.12	6.47
Isoform 3 of Serum albumin	15.76	3.79
Keratin, type I cytoskeletal 14	14.15	7.63
Keratin, type I cytoskeletal 16	10.65	4.86
Endoplasmin	9.89	4.11
Keratin, type II cytoskeletal 6B	9.76	5.32
Keratin, type II cytoskeletal 1b	9.29	2.08
Keratin, type I cytoskeletal 28	8.35	3.45

Table 3-7. nLC-MS/MS-detected proteins in band E (top 30)

Protein	Score	Coverage
Alpha-actinin-4	348.43	73.22
Keratin, type II cytoskeletal 1	319.73	53.57
Isoform ACTN4ISO of Alpha-actinin-4	245.27	69.51
Keratin, type I cytoskeletal 9	223.36	55.06
Keratin, type II cytoskeletal 2 epidermal	223.15	64.48
Keratin, type I cytoskeletal 10	216.60	51.71
Isoform 3 of Alpha-actinin-4	161.91	65.83
Alpha-actinin-1	144.67	30.27
Isoform 4 of Alpha-actinin-1	144.67	29.03
Isoform 2 of Alpha-actinin-1	144.67	30.44
Isoform 3 of Alpha-actinin-1	144.67	29.54
Keratin, type II cytoskeletal 5	117.67	44.41
Alpha-actinin-2	106.28	13.53
Isoform 2 of Alpha-actinin-2	106.28	13.53
Keratin, type I cytoskeletal 14	103.98	48.52
Keratin, type II cytoskeletal 6B	57.10	21.28
Keratin, type II cytoskeletal 6A	55.18	22.87
Keratin, type II cytoskeletal 6C	55.18	22.87
Alpha-actinin-3	52.19	10.43
Hornerin	47.14	14.18
Keratin, type I cytoskeletal 16	46.66	17.97
Splicing factor, proline- and glutamine-rich	46.60	17.68
Keratin, type II cytoskeletal 2 oral	37.32	9.87
Keratin, type II cytoskeletal 75	36.67	13.25
Keratin, type I cytoskeletal 17	35.63	16.44
Isoform Short of Splicing factor, proline- and glutamine-rich	33.28	14.65
Keratin, type II cytoskeletal 3	31.56	7.32
Keratin, type II cytoskeletal 1b	29.00	3.63
Keratin, type II cytoskeletal 8	26.38	7.66
Isoform 2 of Keratin, type II cytoskeletal 8	26.38	7.24

Table 3-8. Genes detected by the shotgun method (top 50)

Ranking	Gene	Score	Coverage	Ranking	Gene	Score	Coverage
1	LMNA	676.95	93.98	26	FAM136A	53.60	80.43
2	PPM1A	429.62	87.43	27	PPM1B	52.19	6.89
3	CTTN	357.62	74.73	28	CALU	51.94	47.94
4	SERBP1	310.59	64.22	29	DHX15	47.99	17.74
5	CLIP2	176.67	57.07	30	SEPTIN7	47.45	37.07
6	PPIA	131.60	84.24	31	MYL6	46.02	83.44
7	ACTB	127.84	50.67	32	RANBP1	45.27	62.19
8	ACTG1	127.84	50.67	33	CLIP1	44.02	15.44
9	ACTN4	118.06	27.44	34	SEPTIN2	43.36	47.37
10	FSCN1	117.90	46.45	35	LMNB1	41.28	20.48
11	ACTA1	95.13	31.03	36	HNRNPA1P48	38.80	38.55
12	ACTC1	95.13	31.03	37	PDLIM5	38.45	16.78
13	ACTA2	93.14	28.12	38	PRDX1	37.46	53.77
14	ACTG2	93.14	28.19	39	RPS12	37.03	67.42
15	CFL1	84.78	79.52	40	HNRNPA3	36.75	24.87
16	CCDC50	84.54	67.32	41	CBR1	36.15	36.10
17	STIP1	82.76	39.96	42	ANXA2	34.55	24.78
18	PKM	79.11	43.13	43	ALDOA	34.12	42.58
19	SEPTIN9	75.96	60.24	44	MYH9	33.85	7.45
20	HNRNPA1	70.88	56.25	45	ACTN2	31.69	7.27
21	WDR1	59.18	46.53	46	TPM3	30.24	43.55
22	ACTN1	55.43	13.34	47	EEF2	28.88	21.21
23	SMAP	55.14	28.42	48	SF3A1	28.67	18.03
24	C11orf58	55.14	33.12	49	SFPQ	27.64	17.11
25	CPOX	55.06	41.63	50	CSRP1	27.30	45.60

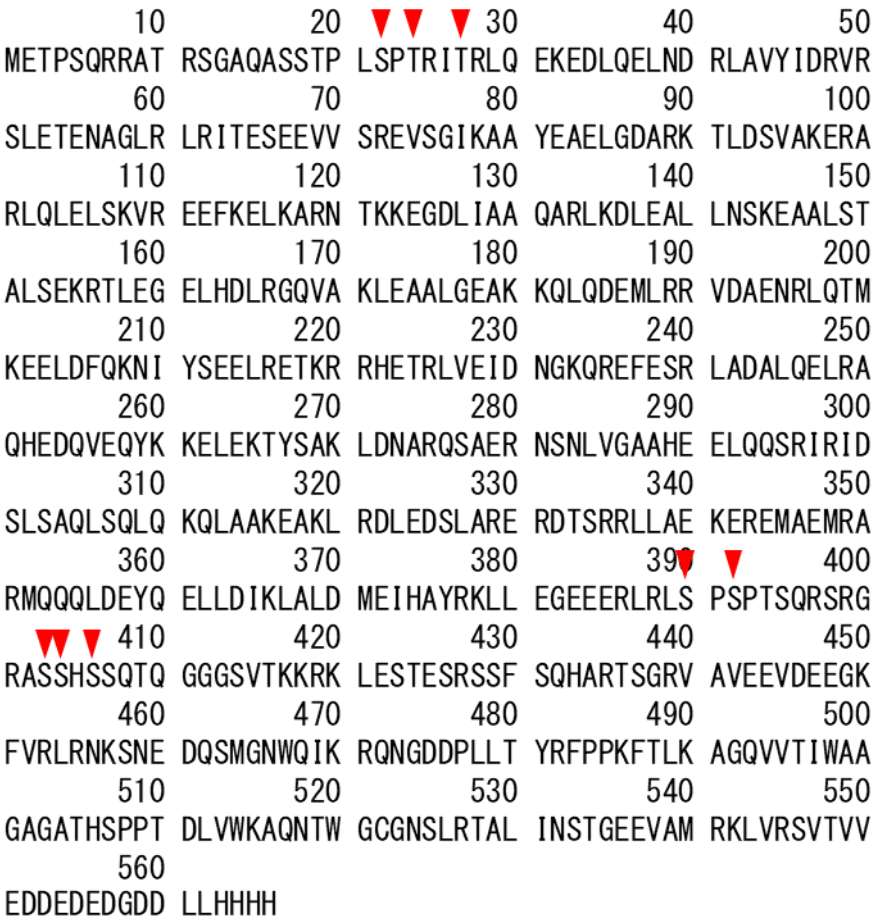

Figure 3-12. Sequence of lamin A/C homologous region (amino acids 1–566).

Eight phospho-Ser and phospho-Thr residues were found in this region (indicated by arrowheads).

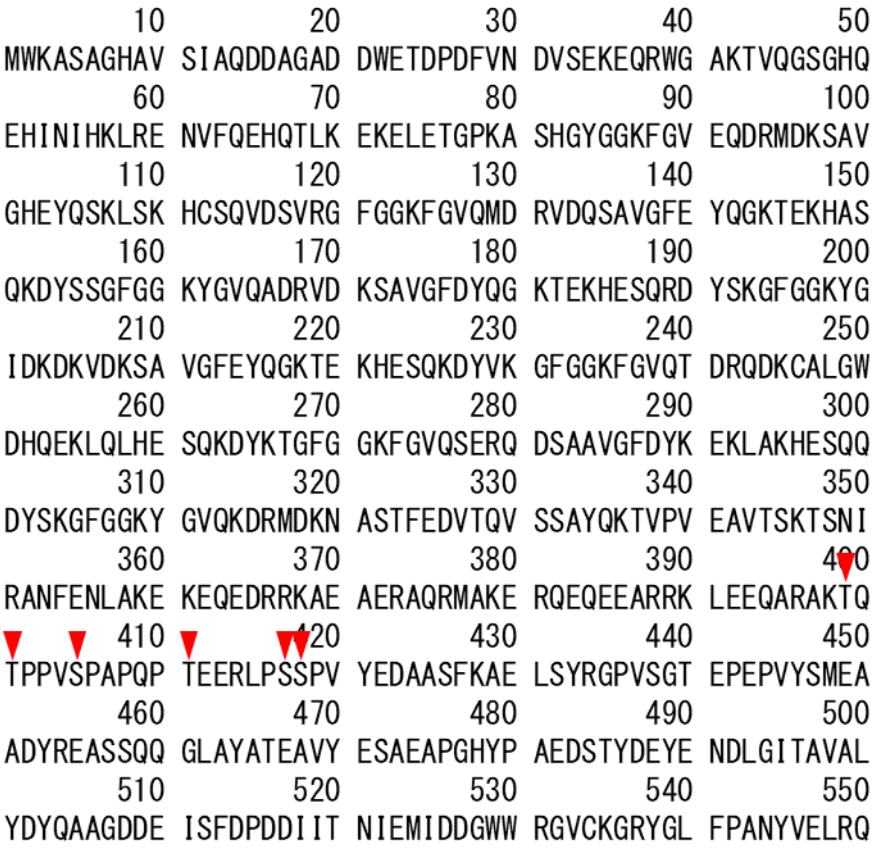

Figure 3-13. Sequence of cortactin.

Six phospho-Ser and phospho-Thr residues were identified in this region (indicated by arrowheads).

3.4.5 Identification of the dephosphorylation site of lamin A/C by PPM1A

To examine the dephosphorylation of phospho-Ser/Thr of lamin A/C and cortactin identified by the shotgun method, *in vitro* phosphatase assay of PPM1A for tri- or di-phosphopeptides containing these phospho-Ser/Thr residues was performed. Lamin A/C(17–32: 22pS, 24pT, 27pT) was highly dephosphorylated, although lamin A/C(385–397: 390pS, 392pS) and lamin A/C (398–411:403pS, 404pS, 406pS) were not dephosphorylated by PPM1A (**Figure 3-14A**). It was also shown that PPM1A dephosphorylates cortactin(394–410: 399pT, 401pT, 405pS) and cortactin(406–423:411pT, 417pS, 418pS). These results showed that lamin A/C and cortactin are candidate novel substrates of PPM1A. Here, we focused on lamin A/C and performed an *in vitro* phosphatase assay for mono-phosphopeptides containing phospho-Ser22, phospho-Thr24 or phospho-Thr27 to examine the dephosphorylation of lamin A/C by PPM1A in detail. Although GST-tagged PPM1A showed no dephosphorylation activity for lamin A/C(17–32: 22pS) at a substrate concentration of 250 μM, lamin A/C(17–32: 24pT) and lamin A/C(17–32: 27pT) were highly dephosphorylated by PPM1A. The k_{cat}/K_m values of PPM1A for lamin A/C(17–32: 24pT) and lamin A/C(17–32: 27pT) were 4.88×10^4 $s^{-1}M^{-1}$ and 2.45×10^4 $s^{-1}M^{-1}$, respectively, which were higher than that of H-p38(176–186: 180pT, 182pY) (k_{cat}/K_m: 2.34×10^4 $s^{-1}M^{-1}$) (**Figure 3-14B**). These results suggested that lamin A/C is dephosphorylated by PPM1A at Thr24 and Thr27.

3.4.6 Dephosphorylation of lamin A/C by PPM1A in cells

In this study, we focused on lamin C as a candidate PPM1A substrate. Because MdST for cell lysates showed that the signal of the lamin C band was higher than that of lamin A, even though both lamin A and lamin C were trapped, one can assume that PPM1A affected lamin C more strongly than lamin A. To confirm lamin A/C dephosphorylation by PPM1A in cells, FLAG3-lamin C was overexpressed in HEK293 cells and phosphorylation of lamin C was evaluated by Phos-tag SDS-PAGE. Lamin C showed various phosphorylation states (**Figure 3-15**). There was less hyperphosphorylated lamin C when PPM1A(WT) was

co-expressed than when PPM1A(D239N) was co-expressed, and the hyperphosphorylation of lamin C(T24A/T27A) was similar in PPM1A(WT) and PPM1A(D239N). This result indicates that PPM1A dephosphorylates lamin C at Thr24 and Thr27 in cells. The phosphorylation state of lamin C in M phase-arrested HeLa cells by nocodazole and in cells after nocodazole release was evaluated because the phosphorylation of lamin A/C is known to be affected by the cell cycle. The signal of the relevant band increased after nocodazole release in lamin C(WT), although no alternative was found in lamin C(T24A/T27A) (**Figure 3-16**). This result suggested that the phosphorylation of Thr24 and Thr27 has roles in mitosis.

3.4.7 Colocalization of lamin C and PPM1A in cells

To examine the role of dephosphorylation of lamin A/C at Thr24 and Thr27, the localization of overexpressed FLAG3-lamin C and PPM1A-HA was observed in HeLa cells. Lamin C was located in the nucleus, and a ring-shaped structure of lamin C was observed in telophase nuclei. PPM1A was located in the nucleus and cytoplasm, and in cells that contained ring-shaped lamin C, PPM1A was accumulated inside the ring. Lamin C(T24A/T27A) and the phospho-mimetic mutant at Thr24 and Thr27, lamin C(T24D/T27D), did not show formation of the ring-shaped structure. PPM1A accumulation was not evident in cells expressing lamin C(T24A/T27A) or lamin C (T24D/T27D) (**Figure 3-17**). The ring-shaped structure of lamin C(WT) was also observed when PPM1A(D239N) was expressed, and PPM1A(D239N) was accumulated inside the lamin C ring similarly to PPM1A(WT) (**Figure 3-18**). These results suggested that the nuclear localization of PPM1A is strongly associated with the localization of lamin C, and that the accumulation of PPM1A inside the ring-shaped structure is independent of its activity.

3.5 Discussion

In this study, PPM1A was selected as the model phosphatase for the development of the MdST method. PPM1A has many roles including in immune response, cell differentiation, and cell cycle regulation (16–19). We proposed a model in which PPM1A recognized various substrate sequences using two Arg residues to interact with the substrate phosphate in Section 2 of this thesis. This suggests that the substrates identified to date are PPM1A substrates.

Here, as a method that can comprehensively identify the substrate of PPM phosphatase, we designed the MdST method in which a stable PPM–substrate complex is formed through the replacement of Mg^{2+} with Zn^{2+} at the active center. *In vitro* phosphatase assay showed that the K_m value of PPM1A was lowest for H-p38(180T, 182pY) and largest for H-p38(180T, 182pY) in three p38 peptides. In GST-PPM1A pull-down with Zn^{2+}, H-p38(180T, 182Y) was the most frequently trapped peptide, while H-p38(180pS, 182pY) was the least frequently trapped among the three p38 peptides. Therefore, it was suggested that MdST with Zn^{2+} is a system that reflects the K_m value for substrates that have the same binding mode. Although the CaMKII peptide had a larger K_m value than H-p38(180pT, 182Y), a larger amount was trapped than H-p38(180pT,182Y). This suggests that CaMKII and p38 have different binding modes.

eEF2, the reported substrate of PPM1A, was trapped in a PPM1A-scpecific manner by MdST from HEK293 cell lysates, indicating that MdST with Zn^{2+} is an effective method for identifying cellular substrates. A large number of proteins previously unknown as substrates for PPM1A were detected by in-gel digestion and the shotgun method. In this study, we focused on lamin A/C, which had the highest nLC-MS/MS score, and identified Thr24 and Thr27 in lamin A/C as substrates of PPM1A.

The band indicated by the arrowhead in **Figure 16** did not have the fastest migration and was increased by the overexpression of PPM1A(WT), indicating that this lamin C species was phosphorylated at sites other than Thr24 and Thr27. This suggested that dephosphorylation of lamin C at Thr24 and Thr27 by PPM1A induced the phosphorylation of other lamin C sites. Phosphorylation of these sites was increased by

stimulation of G2/M cell cycle arrest with nocodazole. It has been reported that lamin C is phosphorylated at multiple sites including Ser22 and Ser392 during G2/M phase and at Thr27 by PLK1. Therefore, it was suggested that the role of PPM1A in lamin C is to promote the phosphorylation of other sites through the dephosphorylation of Thr24 and Thr27. PPM1A is located inside the ring-shaped structure of lamin C in telophase cells. It has been reported that lamin A/C(1–431), which does not contain an Ig fold domain, forms an "intranucleoplasmic ring" in the nuclei of HeLa cells, which is similar to the nuclear structure observed this study (20), but the formation mechanism and functions are unknown. The formation of the ring-shaped structure of lamin C in HeLa cells was independent of PPM1A activity, and the accumulation of PPM1A as bright spots in the nucleus was not shown when lamin C(T24A/T27A) and lamin C(T24D/T27D) were expressed with PPM1A. These findings suggested that the accumulation of PPM1A was induced in a lamin C(WT)-dependent manner and that the phosphorylation of lamin C at either Thr24 or Thr27 is important for the formation of the ring-shaped structure. It is possible that lamin C phosphorylated at either Thr24 or Thr27 accumulates with PPM1A in the ring-shaped structure in telophase and its dephosphorylation by PPM1A occurs after the disruption of the ring-shaped structure. More detailed experiments are needed to clarify the role of PPM1A for lamin C.

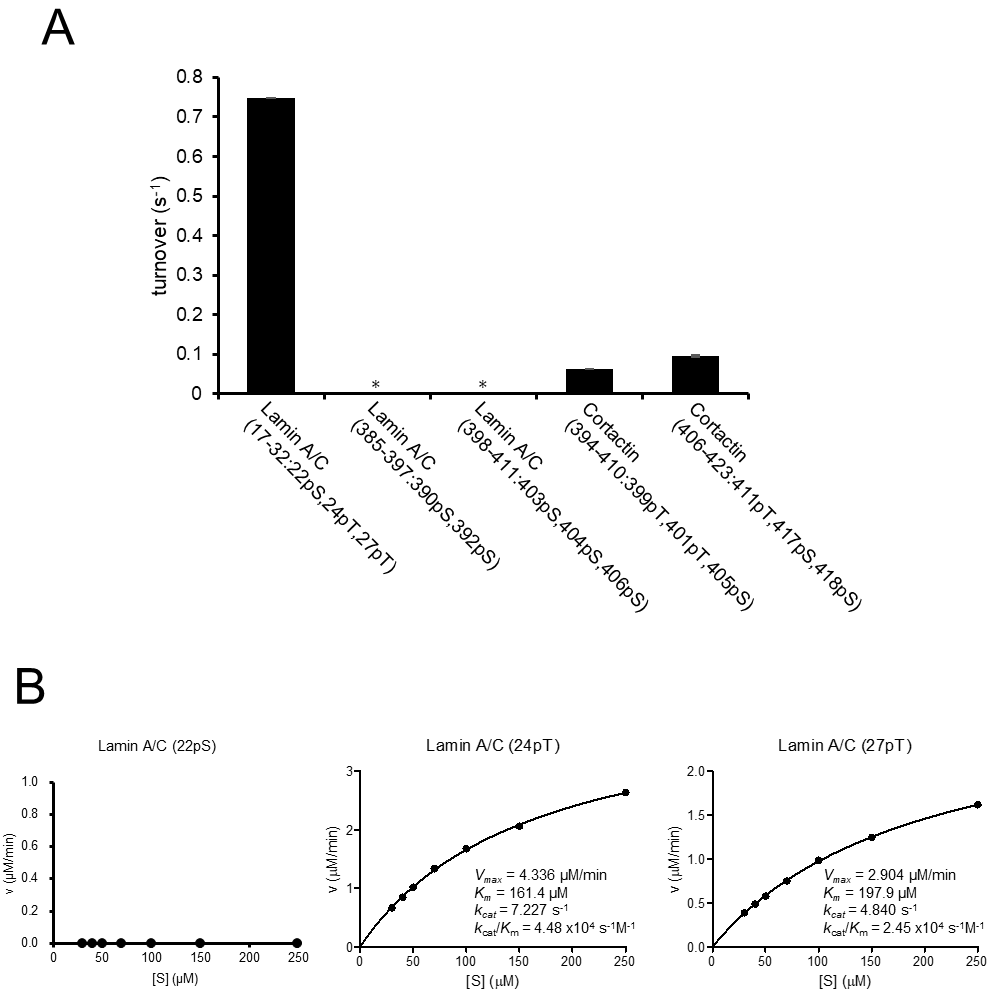

Figure 3-14. Catalytic activity of PPM1A for lamin A/C and cortactin phospho-peptides.

(A) PPM1A activity for tri- or di-phosphorylated peptides of lamin A/C and cortactin. (B) PPM1A activity for mono-phosphorylated peptides derived from lamin A/C 17–32. Experiments were performed in 50 mM Tris HCl pH 7.4, 30 mM $MgCl_2$, 0.02% 2-mercaptoethanol, and 0.1 mM EGTA at 30°C. The data points were fitted to the Michaelis–Menten equation v = Vmax S/(K_m + S) by Prism5 software (Graph Pad Software).

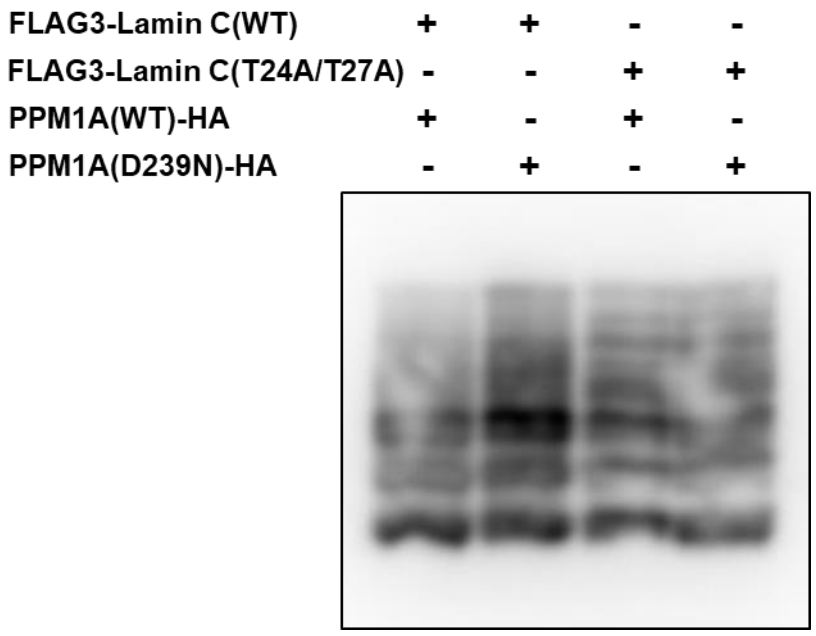

Figure 3-15. Effect of PPM1A on the phosphorylation state of lamin C.

Phos-tag SDS-PGE for FLAG-tagged lamin C(WT) and (T24A/T27A) overexpressed with WT or inactive mutant PPM1A in HEK293 cells was performed, and lamin C proteins were detected by anti-FLAG antibody. The cells were stimulated with nocodazole for 16 h.

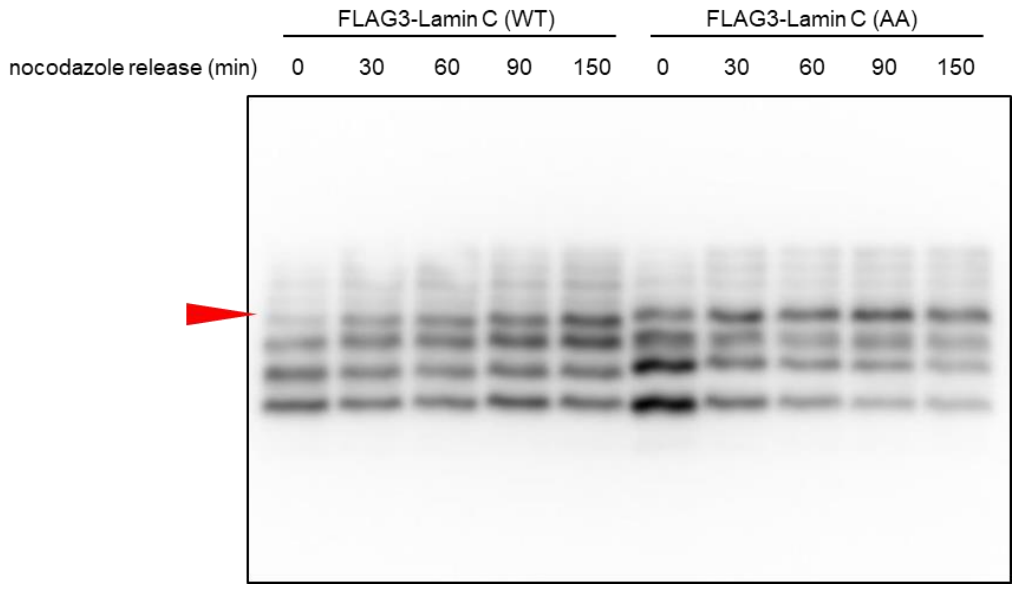

Figure 3-16. Effect of nocodazole release on the phosphorylation of lamin C.

Phos-tag SDS-PGE for FLAG-tagged lamin C(WT) and (T24A/T27A) overexpressed in HeLa cells was performed, and lamin C proteins were detected by anti-FLAG antibody.

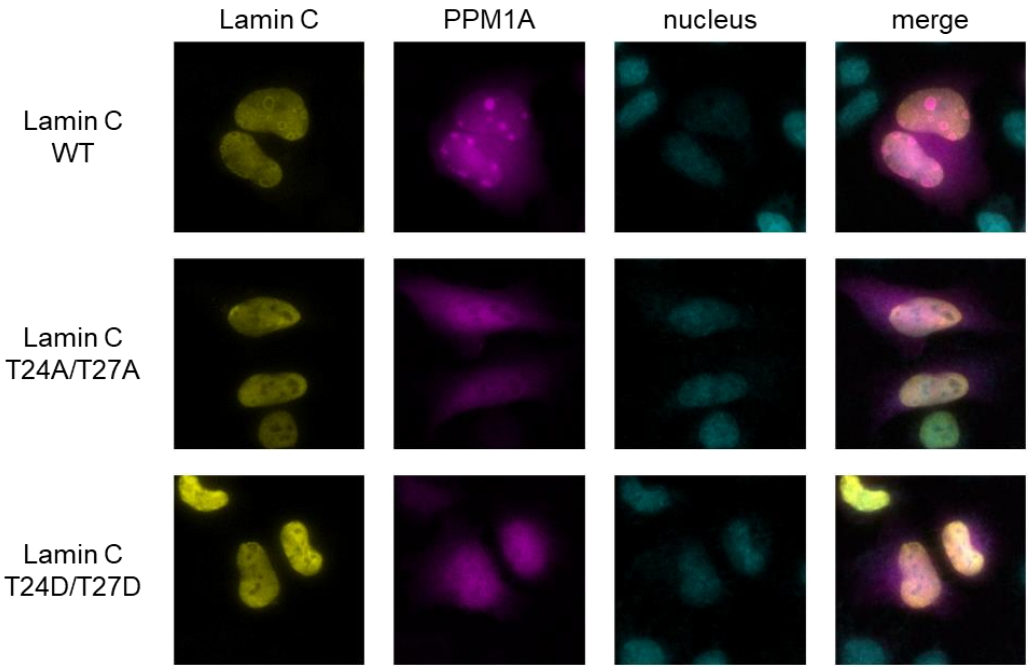

Figure 3-17. Localization of lamin C mutants expressed with wild-type PPM1A in HeLa cells.

FLAG-tagged lamin C and HA-tagged PPM1A were expressed and stained with anti-FLAG antibody and anti-HA antibody, respectively. Nuclei were stained with DAPI.

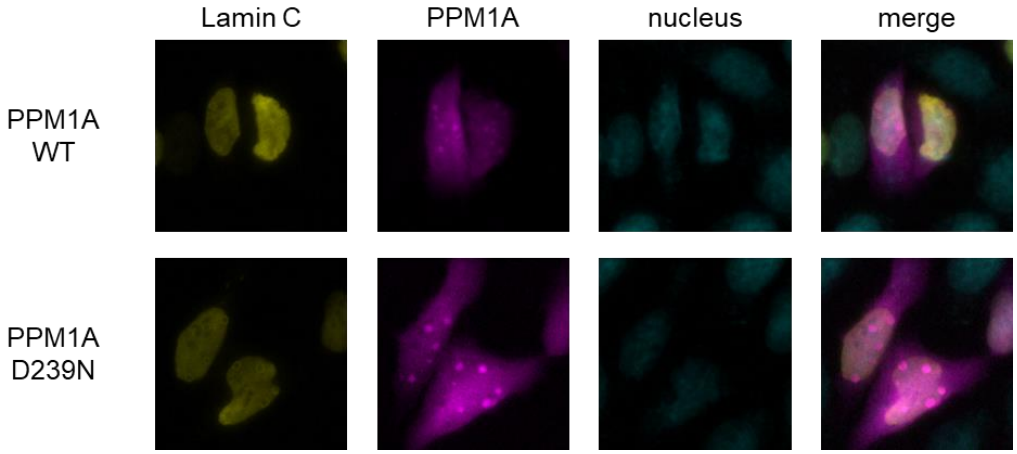

Figure 3-18 Localization of PPM1A mutants expressed with wild-type lamin C in HeLa cells.

FLAG-tagged lamin C and HA-tagged PPM1A were expressed and stained with anti-FLAG antibody and anti-HA antibody, respectively. Nuclei were stained with DAPI.

3.6 References

1. Kamada, R., Kudoh, F., Ito, S., Tani, I., Janairo, J. I. B., Omichinski, J. G. & Sakaguchi, K. (2020) Metal-dependent Ser/Thr protein phosphatase PPM family: Evolution, structures, diseases and inhibitors. *Pharmacology & Therapeutics* **215**, 107622.
2. Das, A. K., Helps, N. R., Cohen, P. T. & Barford, D. (1996) Crystal structure of the protein serine/threonine phosphatase 2C at 2.0 A resolution. *The EMBO Journal* **15**, 6798–6809.
3. Almo, S. C. … Burley, S. K. (2007) Structural genomics of protein phosphatases. *Journal of Structural and Functional Genomics* **8**, 121–140.
4. Wynn, R. M., Li, J., Brautigam, C. A., Chuang, J. L. & Chuang, D. T. (2012) Structural and Biochemical Characterization of Human Mitochondrial Branched-chain ⎵ -Ketoacid Dehydrogenase. **287**, 9178–9192.
5. Gao, C., Cao, N. & Wang, Y. (2021) Metal dependent protein phosphatase PPM family in cardiac health and diseases. *Cellular Signalling* **85**, 110061.
6. Pondugula, S. R., Flannery, P. C., Apte, U., Babu, J. R., Geetha, T., Rege, S. D., Chen, T. & Abbott, K. L. (2015) Mg2+/Mn2+-dependent phosphatase 1a is involved in regulating pregnane X receptor'mediated cytochrome p450 3A4 gene expression. *Drug Metabolism and Disposition* **43**, 385–391.
7. Kumar, A. S., Naruszewicz, I., Wang, P., Leung-Hagesteijn, C. & Hannigan, G. E. (2004) ILKAP regulates ILK signaling and inhibits anchorage-independent growth. *Oncogene* **23**, 3454–3461.
8. Yagi, H., Chuman, Y., Kozakai, Y., Imagawa, T., Takahashi, Y., Yoshimura, F., Tanino, K. & Sakaguchi, K. (2012) A small molecule inhibitor of p53-inducible protein phosphatase PPM1D. *Bioorganic and Medicinal Chemistry Letters* **22**, 729–732.
9. Ogasawara, S., Kiyota, Y., Chuman, Y., Kowata, A., Yoshimura, F., Tanino, K., Kamada, R.

& Sakaguchi, K. (2015) Novel inhibitors targeting PPM1D phosphatase potently suppress cancer cell proliferation. *Bioorganic and Medicinal Chemistry* **23**, 6246–6249.

10. Li, R., Gong, Z., Pan, C., Xie, D. D., Tang, J. Y., Cui, M., Xu, Y. F., Yao, W., Pang, Q., Xu, Z. G., Li, M. Y., Yu, X. & Sun, J. P. (2013) Metal-dependent protein phosphatase 1A functions as an extracellular signal-regulated kinase phosphatase. *FEBS Journal* **280**, 2700–2711.

11. Yamaguchi, H., Minopoli, G., Demidov, O. N., Chatterjee, D. K., Anderson, C. W., Durell, S. R. & Appella, E. (2005) Substrate Specificity of the Human Protein Phosphatase 2C δ , Wip1 †. 5285–5294.

12. Yamaguchi, H., Durell, S. R., Chatterjee, D. K., Anderson, C. W. & Appella, E. (2007) The Wip1 phosphatase PPM1D dephosphorylates SQ/TQ motifs in checkpoint substrates phosphorylated by PI3K-like kinases. *Biochemistry* **46**, 12594–12603.

13. Flint, a J., Tiganis, T., Barford, D. & Tonks, N. K. (1997) Development of "substrate-trapping" mutants to identify physiological substrates of protein tyrosine phosphatases. *Proceedings of the National Academy of Sciences of the United States of America* **94**, 1680–1685.

14. Blanchetot, C., Chagnon, M., Dubé, N., Hallé, M. & Tremblay, M. L. (2005) Substrate-trapping techniques in the identification of cellular PTP targets. *Methods* **35**, 44–53.

15. Wu, D., Wever, V. De, Derua, R., Winkler, C., Beullens, M., Eynde, A. Van & Bollen, M. (2018) A substrate-trapping strategy for protein phosphatase PP1 holoenzymes using hypoactive subunit fusions. **293**, 15152–15162.

16. Budhiraja, S., Ramakrishnan, R. & Rice, A. P. (2012) Phosphatase PPM1A negatively regulates P-TEFb function in resting CD4T+ T cells and inhibits HIV-1 gene expression. *Retrovirology* **9**, 1–10.

17. Dvashi, Z., Shalom, H. S., Shohat, M., Ben-Meir, D., Ferber, S., Satchi-Fainaro, R., Ashery-Padan, R., Rosner, M., Solomon, A. S. & Lavi, S. (2014) Protein phosphatase magnesium dependent 1A governs the wound healing-inflammation-angiogenesis cross talk on injury. *American Journal of Pathology* **184**, 2936–2950.

18. Ofek, P., Ben-Meir, D., Kariv-Inbal, Z., Oren, M. & Lavi, S. (2003) Cell cycle regulation and p53 activation by protein phosphatase 2Cα. *Journal of Biological Chemistry* **278**, 14299–14305.

19. Shohat, M., Ben-Meir, D. & Lavi, S. (2012) Protein phosphatase magnesium dependent 1A (PPM1A) plays a role in the differentiation and survival processes of nerve cells. *PLoS ONE* **7**, 1–11.

20. Duband-Goulet, I., Woerner, S., Gasparini, S., Attanda, W., Kondé, E., Tellier-Lebègue, C., Craescu, C. T., Gombault, A., Roussel, P., Vadrot, N., Vicart, P., Östlund, C., Worman, H. J., Zinn-Justin, S. & Buendia, B. (2011) Subcellular localization of SREBP1 depends on its interaction with the C-terminal region of wild-type and disease related A-type lamins. *Experimental Cell Research* **317**, 2800–2813.

4. Conclusions

Ser/Thr phosphatase PPM family proteins function as monomeric enzymes, unlike other Ser/Thr phosphatase family members. PPMs have various crucial roles including in proliferation, differentiation, metabolism, and immune response, and the abnormal functions of PPMs are reported to cause many diseases such as cancer. However, the substrates of many PPM isoforms are still unknown. This is a major bottleneck in the understanding of the physiological functions of the PPM family. Each PPM phosphatase has an isoform specific N-terminal region, C-terminal region, and loop region, and these isoform-specific regions are important for the regulation of the cellular functions of PPM and for the interaction with their targets. The catalytic domain, whose primary sequence is highly conserved, is important for the recognition of the substrate phosphate group and the adjacent sequences. In the case of PPM1A, substrates with different sequence motifs can be dephosphorylated by PPM1A, but the mechanism of this substrate recognition is unclear. In this study, we revealed the role of two arginine residues in the vicinity of the active center of PPM1A. Furthermore, we developed a novel substrate identification method, "Metal-dependent Substrate Trapping," based on the metal-dependent regulation of PPM activity and identified the nuclear lamina protein lamin C as the PPM1A substrate.

In Chapter 2, we investigated the effect of Arg33 and Arg186 on PPM1A dephosphorylation activity. Gln substitution at Arg33 increased the K_m value and decreased the k_{cat} value of PPM1A for pNPP, whereas substitution at Arg186 had little effect. However, both Gln substitutions at Arg33 and Arg186 significantly decreased the k_{cat} value of PPM1A for the model phosphopeptide Ac-Gly-pThr-Gly-NH_2. Docking model analysis showed that the phosphate group of Ac-Gly-pThr-Gly-NH_2 can be positioned at a distance capable of interacting with Arg186. The substitution at Arg33 and Arg186 showed different effects on PPM1A activity depending on the sequence of the substrate. These observations suggested that both Arg33 and Arg186 interact with the phosphate group of the substrate and that the contribution of these arginine residues on this recognition is different depending on the nature of the substrate. PPM1A has three grooves around the active

center (**Figure 4-1**). In the crystal structure of PPM1A complexed with peptide with the (pT)I(pY) sequence, the side chain of Ile is located at hydrophobic Cleft 1. The residue at P+1 position of p53(20pT) peptide is Asp, and R186Q substitution had a greater effect on activity than R33Q substitution, as with the Ac-GlpThr-Gly-NH_2 peptide. Here, we propose a model in which PPM1A uses these grooves and Arg33 and Arg186, depending on the substrate, to recognize a variety of substrate sequences.

In Chapter 3, we developed a novel substrate identification method for WT PPM and identified lamin C as a novel substrate of PPM1A. In this chapter, we designed the novel substrate identification method "Metal-dependent Substrate Trapping" based on the new principle that Mg^{2+} in the active center of PPM is replaced by inactivating metal ions, resulting in inactive PPM that retains its ability to recognize the substrate to form stable enzyme–substrate complexes. MdST with Zn^{2+} for the phosphopeptide mixture and cell lysate showed that MdST is a highly specific method for the target sequence and that the endogenous substrate can be obtained by this method. In addition, lamin C was identified as a novel substrate of PPM1A. PPM1A dephosphorylated phosphopeptides containing the lamin C sequence with phospho-Thr24 or phospho-Thr27, and the phosphorylation state of WT lamin C in cell was induced to be similar to that of the non-phosphorylated mutant lamin C by overexpression of PPM1A. We found that lamin C forms a ring-shaped structure in cells and that PPM1A is strongly localized in the ring-shaped structure. These results suggested that PPM1A and lamin C interact in M phase cells.

In summary, we revealed the role of two arginine residues that are highly conserved in the PPM family and succeeded in developing a novel substrate identification method that can be applied to all PPM isoforms. This study provides new insights into the mechanism by which PPM proteins recognize their substrates and promotes the elucidation of PPM functions through the comprehensive identification of their substrates.

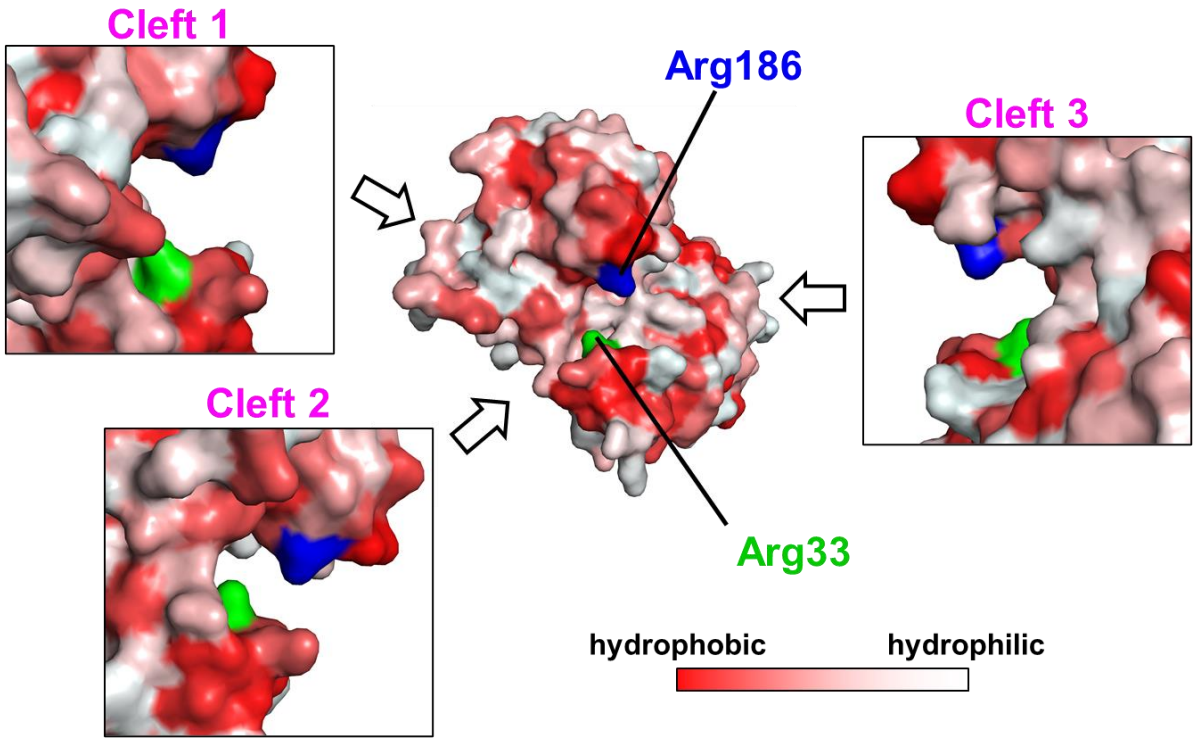

Figure 4-1 Three clefts around the active center of PPM1A.

The surface model of PPM1A (PDB: 6B67) is shown. The three clefts are indicated by the labels.

5. Acknowledgment

I would like to express my greatest appreciation to my supervisor, Professor Kazuyasu Sakaguchi for his guidance and persistent help. Without his generous support, I could not have proceeded with my research.

I would like to offer my special thanks to Professor Yota Murakami (Laboratory of Bioorganic Chemistry), Professor Koichiro Ishimori (Structual Chemistry Laboratory), Professor Tohru Dairi (Laboratory of Applied BioChemistry) and Associate Professor Rui Kamada (Laboratory of Biological Chemistry) for their incisive comments and constructive suggestions on my papers.

I would like to offer my special thanks to Professor James G. Omichinski (University of Montreal, Canada) for his great instruction and advice for my research and paper. I am also very grateful to all the members of the Laboratory of Biological Chemistry. They kindly helped my work and taught me a lot of experimental techniques.

Finally, I would like to offer my special thanks to my family for their constant encouragement and long-term support.